4-21-2017

Study of Damage Progression In CSCM Concretes Under Repeated Impacts

Yevgeniy Parfilko
yvp4331@rit.edu

Recommended Citation

Parfilko, Yevgeniy, "Study of Damage Progression In CSCM Concretes Under Repeated Impacts" (2017). Thesis. Rochester Institute of Technology. Accessed from

Rochester Institute of Technology

Study of Damage Progression In CSCM Concretes Under Repeated Impacts

A Thesis

Submitted in Partial Fulfillment of the Requirements
for the Degree of Master of Science in Mechanical Engineering

In the Department of Mechanical Engineering
Kate Gleason College of Engineering

By
Yevgeniy Parfilko

April 21, 2017

DEPARTMENT OF MECHANICAL ENGINEERING
KATE GLEASON COLLEGE OF ENGINEERING
ROCHESTER INSTITUTE OF TECHNOLOGY
ROCHESTER NEW YORK
CETIFICATE OF APPROVAL

M.S. DEGREE THESIS

The M.S. Degree Thesis of Yevgeniy Parfilko has been examined and approved by the thesis committee as satisfactory for the thesis requirement of Master of Science Degree.

Approved by:

____

Dr. Benjamin Varela, *Advisor, RIT Dept. of Mechanical Engineering*

____

Dr. Hany Ghoneim, *Committee Member, RIT Dept. of Mechanical Engineering*

____

Dr. Sarilyn Ivancic, *Committee Member, RIT Dept. of Mechanical Engineering*

____

Dr. Agamemnon Crassidis, *Department Representative*

Abstract

Reinforced Concrete (RC) is an important material in civil construction projects, and rigorous standards exist for rating the structural, wind, vibration, and cyclic design loads. In narrower applications, such as the design of protective saferooms, RC is also designed to bear impact loads which may be applied repeatedly. Although current experimental and computational methods allow for prediction of concrete damage from a single impact, there is no attempted study of damage progression from repeated impacts. Such a study is attempted on a well-defined slab impact test used in the rating of protection provided by RC walls. Multiple projectiles impact a chosen location and accumulating damage is predicted by means of numerical simulation. The simulation results are then correlated to an experimental test demonstrating similar effects.

The classic projectile impact problem is taken as the basis for computational analysis. Nonlinear wood and concrete material models are substituted for the conventional steel projectile and target, and a damage variable is defined to track cumulative effects of plastic strain. The simulation is then extended to additional impacts while preserving the damaged state of the slab. The development of damage and accumulating strain energy is computed, until damage extends throughout the entire thickness of the slab. Since the contact period per impact is estimated to be under a millisecond, an explicit dynamics formulation of the problem is implemented in commercial software LS-DYNA. The concrete stresses are computed using the Reidel-Hermaier-Thoma Model (RHT), which incorporates a smooth geologic cap model to provide a single continuous failure surface. In this manner, compaction, shear and tensile failures are represented, and consolidated for post-processing by means of a single damage variable.

To verify computational predictions, the impact is recreated experimentally. A set of wood projectiles and RC slabs are fabricated, to allow for repeatable tests. Initial and boundary conditions are recreated by means of a steel bracket for the slab and an air cannon for the projectile. After initial calibration, a repeatable projectile speed, impact location and momentum transfer is achieved. The slabs are impacted repeatedly until macroscopic damage is clearly visible on the front and back faces of the slab. Damaged slabs are then cross-sectioned for material failures and plastic deformation.

The simulations and experimental tests show consistency in predicting the progression of damage in RC slabs. In both cases, through-thickness failure was achieved in 2-4 impacts, depending on the initial kinetic energy of the projectile. Initial damage began as subsurface shear cracking, and in later impacts tensile failures, shear failure (plug formation) and compaction (pulverization) developed concurrently. Granted further verification is performed, there is a promising possibility that these methods and results could be used to provide safety ratings for structures designed to withstand multiple impacts, and to re-asses load ratings of damaged structures more accurately.

Acknowledgements

I would like to extend my gratitude to my advising committee, who have been invaluable mentors to me during this rewarding journey. Dr. Benjamin Varela, Dr. Hany Ghoneim and Dr. Sarilyn Ivancic have provided guidance, patience, and instruction without which this work would not have been possible. Additional thanks goes out to RIT faculty Stephen Boedo and Timothy Landschoot, who have assisted greatly by offering their consultations and lending test equipment. Last but not least, I extend sincerest gratitude to William Finch, Paul Mezzanini, Diane Selleck, Jan Maneti, Rob Kraynik, Kathleen Ellis, and Fernando Amaral de Arruda, for their unwavering support of my efforts, and for transforming the academic environment into a warm, welcoming family. For their love, caring, and years of support, a special thanks goes to my parents Oksana and Vadim, who have given me the motivation and the means to pursue my ambitions.

Table of Contents

List of Figures

List of Equations

List of Tables

Terminology

ASTM	American Society for Testing and Materials
NSSA	National Storm Shelter Association
NDRC	National Defense Research Committee
ACE	Army Corps of Engineers
CEA	Commissariat à l'Energie Atomique
UKAEA	United Kingdom Atomic Energy Authority
BRL	Ballistic Research Laboratory
LLNL	Lawrence Livermore National Laboratory
LSTC	Livermore Software Technology Company

RC	Reinforced concrete
ED	Explicit Dynamics
FEM / FEA	Finite Element Method / Analysis
APDL	ANSYS Parametric Design Language
FFT	Fat Fourier Transform
MIC	Multiple Impact Condition
RHT	Riedel-Hermaier-Thoma [Concrete Material Model]
CSCM	Continuous Surface Cap Model

f_c' = unconfined compressive strengthof concrete in psi

V_0 = initial impact velocity in ft/s

D = damage scaling factor

d = missile diameter in inches

N = missile nose cone shape factor

E = elastic modulus in psi

E_m = elastic modulus of mild steel in psi

W = missile or projectile weight

x = penetration depth

G(x/d) = penetration depth function

1.0 Introduction

Concrete is a hard, brittle material that is present in a variety of structures. It is the oldest engineered structural material, and the first to be used on a large scale in civil construction. Concrete is composed of a hardening cement and a space-filling aggregate. It is known for being a dense, monolithic material that is strong in compression and weaker in tension.

The basic principle of a cement is a hydraulic setting compound, meaning that the cement reacts with water and produces mineral hydrates that act as a binder. Lime, calcium silicate, fly ash, and other mineral compounds can be combined and used as cements. The aggregate that is bound by the cement may be any available material with desirable properties. Sand and gravel are used for construction-grade concrete, while glass, foam or other industrial materials may be used to produce lightweight, heat-resistant, or environmentally friendly concretes. The flexibility of composition results in a range of properties for a wide array of applications, but the mechanical properties of concrete in construction are of primary interest.

The first widespread application of concrete where it was the primary material was the pouring of a load-bearing arch, allowing continuous loading over a span with a discrete number of supports [19]. Domes were an extension of the arch that allowed for the construction of covered buildings and are geometrically complex enough that the use of concrete over worked stone was justified. Additionally, arches had the advantage of creating a purely compressive stress field, thus avoiding concrete’s weaker tensile properties.

Cement was manufactured locally and in small batches, with its chemical composition varying by location. Thus its properties were not significantly repeatable like those of metallic materials. More rigorous manufacturing processes for cements were developed in England in the 18th century, and materials such as Portland cement became common enough to allow a standard of comparison for mechanical properties. The first use of these new concretes was in the laying of foundations for lighthouses on rocky cliffs, where conventional foundations were impossible to construct.

As concrete became more readily available, its uses expanded to a variety of fields, allowing for further innovation. Concrete reinforcement technology was developed in France in the 19th century. Joseph Monier, for example, filed patents for reinforced concrete pipes, beams and bridges between 1868-1878 [19], and his ideas were backed up with engineering data published by Gustav Adolf Wayss. Now that concrete with repeatable properties could be produced and its bearing loads calculated, European engineers began to design bridges, dams and forts with concrete as the primary material.

A common metric to determine the rated strength of concrete is to observe its maximum compressive load in a uniaxial compression test. Today, 2-inch cubes or various size cylinders, as described in the ASTM C109 standard, are used [1]. From the load and geometry, an estimate of the average compressive stress may be obtained, with typical concretes having a strength of 20-35 MPa. The tests, however, do not show the compaction strength of concrete, since the specimen will first fail in tension resulting from the deformation of its free surfaces.

Although buildings such as the roman Pantheon have been known to maintain structural integrity for over 18 centuries, concrete structures that are subjected to impacts and excessive vibrations are at a constant risk of brittle failure. To extend the safety of concrete structures and range of application for concrete, advancements were sought in composites and material science. Reinforcing elements allowed the bearing of tensile loads, while additives gave precise control over properties such as viscosity, settling time, and susceptibility to corrosives. Modern ultrasonic and laser measurement methods enable preventative maintenance, reducing failures greatly. In the present day, concrete is a much more robust material both in terms of load-bearing capability and performance in adverse environmental conditions.

Engineering efforts to completely characterize the mechanics of concrete materials is ongoing. Unlike metals, concretes exhibit complex behavior under strain, including rate-dependent linear deformation, nonlinear plastic deformation, and a variety of fracture modes. The mechanical behavior of concrete was not rigorously quantified until the mid-twentieth century, and various properties such as flame resistance and ecological impact are still being studied in the engineering theory of concretes. These properties are important to consider because they allow the feasibility of concrete application in various unconventional scenarios. Thermal properties of concrete dominate in design of rocket launch pads, for instance, while mechanical fracture is an important consideration for any protective structures or vehicle-related construction. A thorough understanding of these properties is necessary to extend the performance predictions of the structure through its anticipated lifetime.

This work is concerned with a particular type of concrete failure, occurring due to accumulated damage from impacts. This phenomenon, called a multiple impact condition, occurs when an impact load causes localized damage to the concrete, and compounds existing damage from a previous, untreated impact. Section 1.2, research objectives, explains in detail what properties and parameters need to be measured to characterize this type of failure.

1.1 Societal Context

Reinforced concrete found widespread use in civil applications of roads, bridges, dams, docks, canals and protective walls or traffic barriers. Protective structures commonly utilize some form of reinforced concrete. As a consequence of its long lifespan, concrete is expected to protect against many instances of damage, including crashes or ballistic impacts.

Proper characterization of concrete damage and its effect on the service life of concrete is crucial to engineers that set design and maintenance goals for the structure. Understanding the dynamic behavior of concrete materials under impact will result in better-designed structures, which will in turn minimize civilian injuries. Similarly, understanding the damage progression in concrete will result in better assessment of damage zones after the impact has taken place.

As performance and rigor of design continue to increase, proven design paradigms may be incorporated into codes and standards that guide the development of future projects. At the present time, additional research work will be necessary in order for the standards to be representable of a variety of scales and input conditions [12].

1.2 Research Objectives

The primary research question is to characterize the repeated impact phenomenon. Since repeated impacts have not been studied from a perspective of structural codes and standards, several derivative implications are to be considered in addition to the main research question:

- What are the transient dynamics of a missile impact into pre-damaged concrete? Specifically, what are the stresses, strains, contact pressures, and accelerations of material elements within the immediate impact zone? How do finite element predictions compare to experimental data?
- Can existing empirical and numerical models in published literature be extended to predict accumulating damage from repeated impacts? If they can, how accurate are the predictions relative to the prediction from initial impact? If they cannot, how may an accurate prediction model be constructed from experimental data?
- How can the insight into behavior of pre-damaged concrete be incorporated into safety standards to make them more comprehensive? Can a structure be designed to withstand a minimum number of consecutive impacts rather than a single impact? Alternatively, can a non-intrusive inspection be used to determine a repair procedure to return structural integrity, given a period of potential exposure?

In order to answer the research question, itemized objectives are set forth to allow the study, data collection, analysis and review of the repeated concrete impact experiments. The following section lays out the format of this work and describes how each section supports the investigation of the research objectives.

1.3 Scope of the Present Work

- To study the transient dynamics of a missile impact into pre-damaged concrete, a robust, efficient finite element model is developed. The model consists of one or more impacting masses and a constrained concrete specimen. Stress, strain, contact pressure, and local accelerations in the impact zone will be simulated.

- The design and characterization of the experimental setup will be conducted based on the predicted results of the finite element simulation. The type, quantity and placement of proper sensing equipment will be derived from the computational model, to allow analogous data to be collected. The initial conditions will be supplied by a projectile acceleration system, and the boundary conditions will be met by means of a rigid support.

- The experimental setup and proper measuring equipment will be fabricated in four sections: an air cannon to launch and measure the speed of soft projectiles, a set of concrete slabs with accelerometers, a set of projectiles, and a constraining bracket. The experimental setup will be designed to be reusable, except for the concrete specimens.

- Experimental tests will be executed to replicate and validate the simulations. Acceleration data will be recorder in real time, and the concrete material will be inspected after each impact to obtain plastic deformation and damage measurements. The geometry of the cracks will be measured and compared to previous instances to infer the propagation.

- The data obtained from experiment will be compared to numerical models, and if possible, fit to the respective model parameters to show how repeated impacts relate to one-time impacts.

2.0 Literature Review

Over the 150 years since the industrial revolution, concrete has been used for industrial, defensive, aesthetic and commercial projects on a variety of scales. During this time, analytical methods, design standards, and experimental tests for concrete structures underwent significant changes. The progression of these methods within the context of application will be summarized thoroughly and concisely in the literature review section.

2.1 A history of concrete design for ballistic impacts

2.1.1 Early military applications

Concrete, along with other forms of masonry, has been used in a variety of structures ranging from aqueducts to temples to protective walls. These historic structures were designed to bear a static load, most of which was the material weight. Transient loads were addressed by incorporating a large factor of safety. Thus, the primary engineering effort was to ensure the structure could support its initial load. The first consideration of external impact loading stemmed from the problem of designing an economical protective military structure to be able to withstand the transient load from a ballistic projectile. Initial work specifically addressed dull-nosed steel artillery shells. However, the strength of the pour depended heavily on the quality of the cement and the workmanship; the strength of a structural pour was not yet repeatable.

In the beginning of the twentieth century, concrete technology had developed enough to allow large-scale civil engineering projects. The first publication to rely on experimental data in quantifying the protection provided by a barrier was conducted by Petry in 1910 [26]. Petry assumed a solid steel projectile and a semi-infinite concrete barrier, such that the missile could never break through to the other side.

$$X = 12\, K_p A_p \log_{10}(1 + \frac{{V_0}^2}{215000_{ft/s}})$$

Equation 1. Petry I equation as given by Amirikian [4].

Based on ballistic impact tests, Petry was able to establish a logarithmic correlation of the kinetic energy of the projectile (given by the squared velocity term, and normalized to a reference velocity) to the relative depth of penetration (given by X). Linear constants A_p and K_p allowed the prediction to account for the frontal weight-per-area of the missile and material property constant of the concrete, respectively. Table 2.1 shows each variable, its description and units.

Table 2.1. Input/output parameters for the Petry equation [13].

Variable name	Symbol	Units	Ref. value
Depth of penetration	X	ft	0.0100
Concrete material penetration coefficient	K_p	-	0.0083
Missile weight per projected area	A_p	lb/ft^2	600
Impact velocity	V_o	ft/s	450

This equation was not dimensionally accurate, and was a simple fit of a logarithmic law to test data; the corresponding report was published as a “Monograph on Artillery Systems” [26]. Not surprisingly, little academic progress was made over the next forty years, and the next landmark work to be published in the field was authored by U.S. naval head design engineer Arsham Amirikian in 1950 [6]. Amirikian references the work of Petry, and derives a graphical representation of the Petry equation. However, he writes in his report, “Design of Protective Structures”, that determining penetration depth beyond a rough estimate is of little practical interest due to the variety of factors that control impact speed and force. Rather than offering a single equation for concrete barriers, Amirikian introduces several approximations for solid missile impacts and various blast loads, and bases the concrete dimensions on heuristic estimates of a factor of thickness. For instance, he illustrates that for a 2,000 lb. explosive charge impacting at a terminal velocity of 1,000 ft/s, the depth of impact is predicted to be 1.34 feet due to the explosion energy and 3.15 feet due to the kinetic energy. He then suggests a design with a double ceiling of 6 feet and 4 feet, respectively, to absorb the two energies independently. This type of estimation is consistent with the conservative design philosophy employed by military engineers, where there was a continued risk of weapons technology advancing unexpectedly. The recommendation also shows that protective structures of the time were designed to withstand a single, head-on impact and did not make any provisions for the assessment of damage and ultimate repair of the construction.

Meanwhile, in the 1940s the National Defense Research Committee was tasked with conducting extensive experimental tests to determine the penetration capabilities of more modern ballistic missiles, which were known to reach speeds up to 3000 m/s. Data sets from about 900 missile tests were subsequently summarized by curve-fit equations, and are generally known as the NDRC equations [13]. They became widely used in the 1950s due to their closed form and straightforward simplicity. Rather than relying on precise missile characterization, the NDRC equations made up for unforeseen parameter variation by giving conservative estimates of required concrete thickness.

$$G\left(\frac{x}{d}\right) = \frac{180}{(f_c{}')^{0.5}}\, N\, D\, d^{0.2} \left(\frac{V_0}{1000}\right)^{1.8} \quad ; \qquad G\left(\frac{x}{d}\right) = \begin{cases} (\frac{x}{2d})^2 \; for \; \frac{x}{d} < 2 \\ \frac{x}{d} - 1 \; for \; \frac{x}{d} \geq 2 \end{cases}$$

Equation 2. NDRC equations as given by Teland [30].

The equation differs from the Petry equation in several respects. Most notably, the compressive strength of the concrete is a direct input parameter rather than the specific weight constant used by Petry. The equation also considers two cases of penetration, described by the function G(x/d). In one case, the penetration depth is less than twice the projectile diameter, and in the other case the penetration is deeper. This addressed the different behavior of thin, piercing missiles in use at that time. The non-integer exponents of the equation are the result of statistical regression methods that were used estimate the parameters based on the test data. A description of the equation variables is given in Table 2.2.

Table 2.2. Input/output parameters for the NDRC and Kar equations. [13].

Variable name	Symbol	Units	Ref. value
Normalized depth of penetration	x/d	ft./ft.	
Concrete compressive strength	f_c'	psi	3000
Nose cone shape factor	N	-	1.0
Missile weight	W	lb.	50.0
Missile diameter	D	in.	4.0
Impact velocity	V_o	ft/s	450
Elasticity ratio (material to mild steel)	E/E_m	psi/psi	1.0

To summarize, various military engineers laid the groundwork for evaluating concrete impacts. Perty introduced the method of impact testing, while Amirikian was able to derive some general guidelines for estimating impact loads based on missile parameters. The NDRC was able to supply more extensive test data and a more refined set of formulas. Despite these improvements, the scope of the work was narrowly focused on the design of bunkers and missiles, with no consideration for repair or extended service life.

2.1.2 Civil Applications

In the years after the Second World War, design considerations shifted away from preventing missile penetration, and focused on civil applications. Rapid growth of suburbs created an enormous demand for concrete in roadways, bridges, dykes, tunnels and barriers. Energy infrastructure hubs such as power plants still needed protective enclosures however, and these were now required to serve a much longer life. These structures needed to be economical and withstand multiple modes of failure – scabbing, spalling, weathering – instead of simply lasting through a one-time ballistic impact.

This trend was reflected in the research on concrete, as witnessed by several studies into optimizing concrete designs. Since concrete structures were now designed to last decades rather than months, more subtle forms of wear and weathering were being taken into account. Consulting engineer A. K. Kar [17], for instance, conducted a comparative study on the effect of softer, lighter projectiles into concrete structures, such as those imparted by tornado-accelerated debris. He implemented a modified NDRC formula and included a term to scale the penetration depth of projectiles based on their elastic modulus relative to mild steel.

$$G\left(\frac{x}{d}\right) = \frac{180}{(f_c{}')^{0.5}} \left(\frac{E}{E_m}\right)^{1.25} \frac{W\,N_2}{D\,d^{1.8}}\left(\frac{V_0}{1000}\right)^{1.8} ; \qquad G\left(\frac{x}{d}\right) = \begin{cases} (\frac{x}{2d})^2 \; for \, \frac{x}{d} < 2 \\ \frac{x}{d} - 1 \; for \, \frac{x}{d} \geq 2 \end{cases}$$

Equation 3. Kar Formula for penetration from tornado-generated missiles [30].

The Kar equation has the same proportional relationships as the NDRC equation, and makes the additional assumption that penetration from projectiles less dense than steel will scale according to a power law. The significance of this term is that, in addition to allowing a missile of any material, the analyst might now be able to derive an elastic modulus of a composite assembly, such as a vehicle. Studies conducted by engineers such as Kar generated a fair amount of experimental data on concrete impacts, and gave concrete manufacturers, as well as structural engineers, access to a variety of simple, closed-form formulas that accelerated design calculations. A majority of these formulas were developed from 1975 to 1999; a selection of formulas and their years of publication is given in Table 2.3. Although they were simple to use, researchers developed them independently and with regard to a specific applications or datasets. Thus, the use of multiple formulas when designing for complex failure conditions was not practical, as the penetration predictions for each formula varied substantially. A certain degree of intuition was required to know which formula would best match an experimental application, as noted by later researchers [32].

Table 2.3. Summary of published formulas to predict missile penetration into concrete or geopolymer materials [30].

Formula Name	Pub. Yr.	Purpose
Army Corps of Engineers Formula	1946	Military & civil construction
Adeli and Amin Formula	1984	Best polynomial fit
Ammann and Whitney Formula	1976	Explosive fragments
Bechtel Corporation Formula	1976	Scabbing prediction
Bergman Formula	1949	Based on Beth formula
British Formula	1988	Weapons penetration
Ballistic Research Lab Formula	1969	Perforation – ballistics
CEA-EDF Formula for Perforation	1977	Perforation – nuclear reactor
Chang Formula	1981	Perforation and scabbing
CKW-BRL Formula	1982	Semi-infinite targets
Forrestal Formula	1994	Semi-analytical derivation
Haldar and Miller Formula	1982	Nuclear reactor protection
Hughes Formula	1984	Neglects scabbing/perforation
IRS Formula	1984	Crater prediction
Kar Formula	1978	Tornado generated missiles
Kar Steel Target Formula	1968	Low velocity impacts
McMahon, Meyers and Sen Model	1979	Soft Impacts
Barr, Carter, Howe, and Nielson Formula	1980	Structural impact
Modified NDRC Formula	1946	Ballistic missile penetration
Petry Equation	1910	Projectile penetration
Perry and Brown Formula	1982	Pre-stressed slabs
Stone and Webster Formula	1976	Scabbing
Takeda, Tachikawa and Fujimoto Formula	1979	Hard impacts
British Textbook of Air Armament Form.	1955	Aggregate size dependence
Tolch and Bushkovich Formula	1947	Penetration into rock
UKAEA Formula	1990	Nuclear reactor protection
Young Formula	1996	Penetration mechanics course

2.1.3 Modern applications

Today, certain protective structures continue to be designed to prevent penetration of various projectiles. Government buildings and nuclear fuel storage facilities, for instance, are often designed to withstand commercial airplane crashes [16]. Roadside barriers and various transportation-related structures are designed to withstand a glancing vehicle collisions [21] [5]. Tornado saferooms are designed to protect against debris, wind, or falling trees [24] [25].

Due to the varied nature of the scale, geometry, and environmental conditions of these problems, little analytical work is done to generalize the concrete behavior beyond the scope of its application. Instead, the structural soundness is verified by commercial and proprietary finite element programs, and empirical equations are only used to set bounds for design parameters. The advantage to the use of finite element models over empirical equations is that only local failure of any given element is considered, and the global depth of damage or penetration is a result of running a simulation with the desired mesh and initial conditions. In this way, damage on surfaces with non-standard boundary conditions may be found, or missiles with non-standard geometry may be studied. The main disadvantage of this method is the computational cost.

2.2 A history of computational analysis of impacts

Weapons technology advanced significantly during the cold war era, and the proliferation of nuclear missiles introduced a completely new set of defense criteria. Rather than dissipating the momentum from a point load, a concrete shelter could now be subjected to a propagating shockwave. This necessitated an analysis technique known as explicit dynamics, where the dynamic state of a system is solved for by numerical extrapolation over a small time step. Because this technique used a discretized time domain, it made sense to use a discretized spatial domain as well, in the form of a finite element formulation of the dynamic system.

The first research organization to achieve an explicit dynamics solver for 3-D finite element problems was the Lawrence Livermore National Laboratory (LLNL). A solver called DYNA-3D, written by Dr. John O. Hallquist [15] in 1976, was used for the assessment of the effectiveness of atomic weapons systems. It was also the first 3-D FEA solver to incorporate general single surface contact [8]. Later development of DYNA-3D focused on computational efficiency of elements and advanced material models for the medical, automotive and aerospace industries. In 1987, Livermore Software Technology Company (LSTC) separated from LLNL and DYNA-3D became the commercial code LS-DYNA. Figure 2.1 shows a visualization of an explicit dynamics solution.

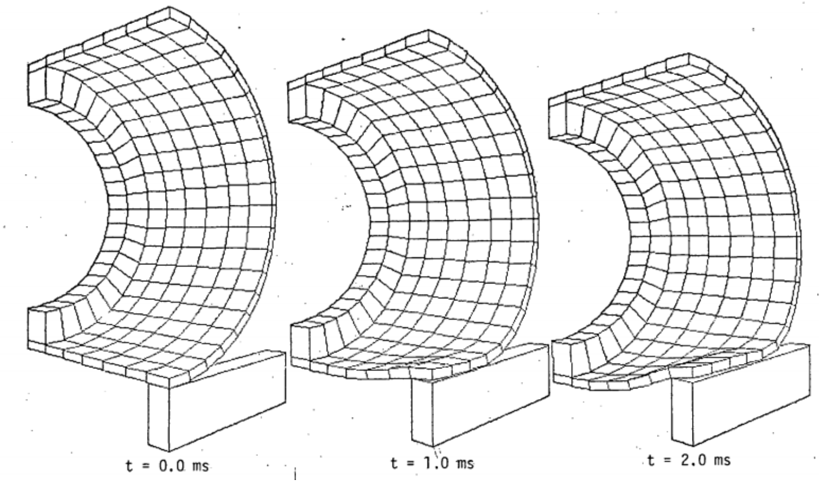

Figure 2.1. A sample 3-D problem solved by DYNA-3D. The program was capable of capturing large deformations over small timescales, and included robust contact algorithms [15].

In the figure, a hollow cylinder is impacted by a bar along its plane of symmetry. The resulting deformation takes place over 2.0 milliseconds and results in partial buckling of the cylindrical surface, as well as the conformance of the pipe to the shape of the bar. Such a problem would be considered to have large deformations in solid mechanics, which, along with the necessity of including plastic strains and inertial effects, would have made the solution complicated. LS-DYNA was the first software to solve such contact problems efficiently and accurately.

Following the development of LS-DYNA, numerous other FEA software packages became available for academic and industrial use. Among those used for dynamic simulations of concrete is ANSYS Mechanical APDL, Dassault Systems ABAQUS, VecTor3 [27], as well as proprietary code and material models from Sandia Labs [14]. This work relies primarily on material models available in LS-DYNA. The evolution of these models is summarized in the next section.

2.2.1 Concrete material models

The first concrete-like material models in LS-DYNA were incorporated to study shockwave propagation through concrete structures [15]. Examples include MAT_SOIL_AND_FOAM and MAT_PSEUDO_TENSOR [4]. The latter incorporated a piecewise failure surface, shown in Fig. 2.2.

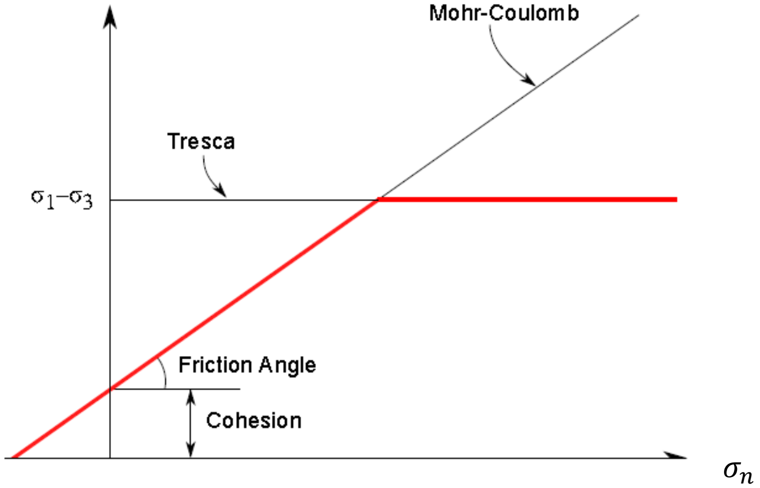

Figure 2.2. Limit surface of MAT_PSEUDO_TENSOR on the normal-shear plane [4].

The figure shows stresses in the normal-shear stress plane. The slanted line represents a brittle failure as predicted by the Mohr-Coulomb criterion. The Tresca criterion represents the maximum shear stress that concrete could bear, and is shown by the horizontal line. The combination of these gives the failure surface, shown by the bolded line. It is noteworthy that this model does not predict compaction, since compaction is of concern only in the immediate vicinity of the impact. Additionally, the shear failure mode is dominant, since the material may fail in tension only if no shear stresses are present. The model incorporates several modifiers that allow the manual adjustment of certain behaviors, such as strain hardening or softening and damage scaling. These modifiers were a great milestone in creating a robust material model, but had limited application to real-world applications since every parameter had to be manually defined, even if it was impractical to test for the value of such a parameter in a test sample.

A significant improvement in the accuracy of geomaterial models was achieved in 1979 with the development of the Geologic Cap Material Model (LS-DYNA MAT_GEOLOGIC_CAP _MODEL) by Sandler and Rubin [28]. This type of material had a distinctly different failure envelope from linear materials, incorporating a tension and compression cutoff as shown in Figure 2.3. The cap surface allowed the material to fail in compression as well as shear and tension, leading to more realistic behavior under complex loading. Specifically, failure modes such as compaction and kinematic hardening allowed for pulverization and realistic hysteretic energy dissipation. This was the first step to incorporating fatigue effects into concrete modeling.

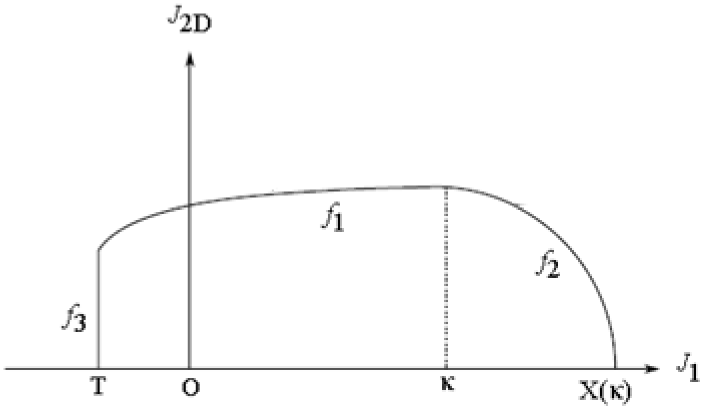

Figure 2.3. Geologic CAP model by Sandler and Rubin, defining tensile and compressive failures [28].

In the figure, the failure surface is composed of three piecewise functions plotted on the isobaric-deviatoric plane, denoted by invariance coordinates J_1 and J_2. The first part, f_1, is a square root law relating J_1 and J_2, more closely fitting the nonlinear deviatoric failure surface. The second piecewise failure surface is the hardening cap, f_2, representing compressive failure. This is given as a function of J_1 and kappa, an internal history variable that tracks accumulation of volumetric strain. The third, f_3, is a tensile cutoff surface which is independent of J_2. The physical significance of the tensile cutoff is a loss of shear strength after a certain tensile strain, even if the Mohr-Coulomb criterion is not exceeded.

In the 1980s, various concrete models continued to be developed to simulate specific behaviors. The Winfirth concrete model could track and display vector fields of the crack orientation [23] and could simulate cracking damage due to an explosive charge. While these improvements modeled concrete materials under specific testing conditions, their generalization was limited because failure modes remained discontinuous, meaning that multimodal failure was not accurately represented. This limited the applicability of discontinuous boundary conditions, especially in the case of steel reinforcement. The challenge was circumvented by averaging the mechanical properties of steel and concrete to create a “smeared” material along the desired plane of reinforcement [29]. Concurrent research in the US and Germany aimed to overcome this limitation via the introduction of a more general failure surface.

In 1999, a new concrete model was developed at the Ernst Mach Institute. It incorporated a continuous failure surface, and was generally applicable to penetrations, explosive charges, compaction and multimodal failure. Named after researchers Reidel, Hermaier and Thoma, the RHT Concrete Model was used for some time as a stand-alone numerical code. This model offered a comprehensive set of equations covering nonlinear behavior of concrete, strain rate effects, erosion criteria, thermal effects, dynamic damping and porosity effects. Its range of application included simulations of subsonic and supersonic impacts, explosive charge detonations, shear failures, and dynamic responses to earthquakes. In 2011, the material became available in the default LS-DYNA library as LS-DYNA MAT_RHT [9].

In 2007, the US Department of Transportation in conjunction with APTEK published a comprehensive concrete model that was based on 14 years of defense research contracts [21]. Instead of using three piecewise limit surfaces, the model utilized a continuously differentiable function for its yield and failure surfaces. The Continuous Surface Cap Model (CSCM) became incorporated into LS-DYNA as MAT_CSCM. Because the failure surfaces were continuous, smooth transitions from one failure more to the next could be achieved. This allowed excellent smoothness of results even with coarser meshes, and also allowed modeling of line elements representing embedded steel reinforcement. In figure 2.4, a visualization of the failure surface is shown on the isobaric-deviatoric plane, with coordinate axes labeled pressure and shear. The continuous function is the combination of an exponential cap function subtracted from a linear (Mohr-Coulomb) function. Although the failure surface is not derived from analytic relationships, it closely approximates test data and is computationally implementable. The linear-exponential surface is described by four parameters: tensile strength, compressive strength, shear strength or cohesion, and an exponential coefficient for the shape of the cap.

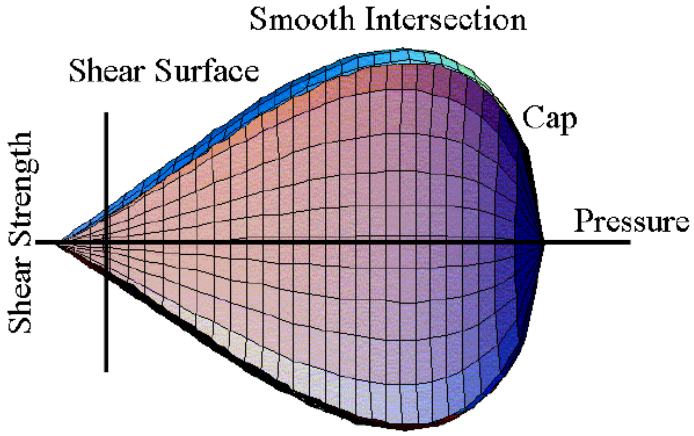

Figure 2.4. Continuous Surface Cap as used in MAT_CSCM [19].

Overall, the proliferation of computer simulation in engineering analysis led to the creation of a variety of specialized software codes and material models. Like empirical equations, all numerical models make the tradeoff between computational efficiency and prediction accuracy. However, most numerical codes offer a great range of parameters that can be tuned to the specific application of simulation, and the user often has the choice of selecting only the necessary parameters for the desired complexity of material response [14]. Thus, material efficiency and accuracy is always optimized.

Previous research efforts have compared the performance of numerical models given the same input problem [10]. The author conducted a brief independent survey of 19 numerical models available in commercial and proprietary software. The models are summarized in Table 2.4.

Table 2.2. Summary of published numerical models of concrete and geological materials [4].

Model Name	Purpose	Implementation
ANACAP Concrete	General / Industry consulting	ANTECH
BF1 Geomaterial	Research / Defense	Sandia Labs
Concrete Damage Rel.3	General / Industry consulting	LS-DYNA 072
Concrete Beam	Structural analysis	LS-DYNA 195
Concrete EC2	Structural analysis (Eurocode)	LS-DYNA 172
Continuous Surface Cap Model	USDOT Roadside Structures	LS-DYNA 159
Concrete Damage Plastic Model	Failure w/ dynamic loading	LS-DYNA 273
Drucker-Prager Cap Model	Soil modeling	LS-DYNA 193
Gebbeken-Ruppert Concrete	Explosive charge modeling	Autodyn2D
Geologic Cap	Multimodal failure modeling	LS-DYNA 025
Johnson-Holmquist Concrete	High-strain applications	LS-DYNA 111
Oriented Crack	Fracture and tensile failure	LS-DYNA 017
Pseudo Tensor	Reinforced concrete shock	LS-DYNA 016
RHT Concrete	Impacts and explosive charges	LS-DYNA 272
Schwerr Murray Cap Model	Geomaterials with viscoplasticity	LS-DYNA 145
Smeared Crack	Cracks in isotropic materials	LS-DYNA 131
FHWA Soil	Roadbase soils	LS-DYNA 147
Soil Concrete	Efficient concrete and soil model	LS-DYNA 078
Winfrith Concrete	Reinforced concrete slab w/crack	LS-DYNA 084

2.3 Experimental Failure Modes

Design loads that a concrete structure bears may be generally categorized as static, dynamic or shock loads. Examples of static loads are concrete beams in bending, or concrete slabs bearing distributed loads. Concrete cantilevers under cyclic loading may be said to be dynamically loaded. Shock loadings, on the other hand, deal with a much more rapid transfer of energy and momentum, and may be due to ballistic impact, explosive charges, or an inertial impulse.

For concrete slabs loaded at the center and supported at the corners or sides (as illustrated in Figure 2.5 A), existing research describes several qualitatively different failure modes [22]. The most drastic type of failure, seen in cases of high-density impacts [11] or explosive detonations [9], is that of plug formation. In this mode of failure the load is applied rapidly, and shear stresses develop between the area under the footprint of the missile or charge and the free surface of the slab. Cracks initiate near the top surface around the footprint, and propagate down at an angle to the back face. The resulting truncated cone, called a plug, separates from the bulk of the slab. This type of damage occurs immediately after impact, along the front of the primary shockwave. It is illustrated in Figure 2.5 B.

For ballistic impacts at lower velocities, or for soft (deformable) projectiles, the contact time may be somewhat longer, and the slab may begin to deform globally as well as locally. In this case cracks will form in the tensile region of the slab, as shown in Figure 2.5 C. As the slab continues to bend, the crack propagates upward to the front face. This is the primary mode of failure for reinforced beams and walls impacted by a distributed load, and existing research [31] correlates well to crack-based damage models of concrete [29]. Some thin slabs, however, may still experience plug formation [32].

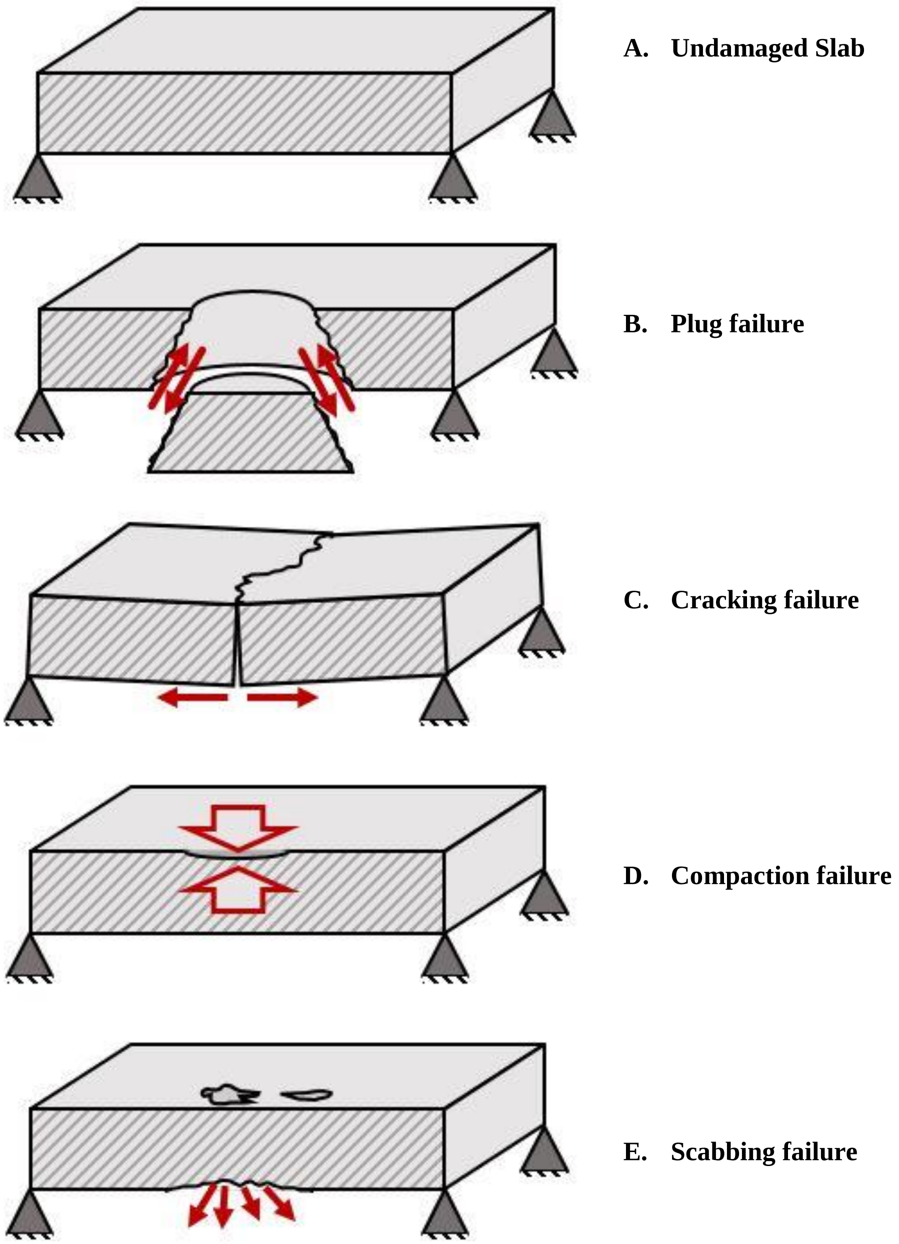

Figure 2.5 - Illustration of four common failure modes of concrete. Failure modes may occur independently, or together.

As the missile mass is decreased relative to the concrete slab, or the stiffness of the concrete structure is increased by means of geometry or scale, impacts may not cause extensive damage. Instead, the concrete may become compacted under the projectile or a pressure wave may cause scabbing and spalling around the projectile, as show in Figure 2.5 D and E, respectively. These two modes of failure do not threaten the structural integrity of the test specimen, but they are important to consider for a multiple impact condition because of the high probability these sites of local damage may become crack nucleation zones. In cases where concrete subjected to cyclic loading, scabbing and spalling are indicators of zones of higher strain and softening.

It is not always clear which failure mode will be the dominant one for a given impact scenario. Thinner slabs tend to fail by plug formation, while slabs that act as beams tend to crack. Any concentrated load from a sharp projectile may also cause scabbing and compaction. For slabs whose geometry does not fall into definite categories, failure modes occur concurrently, or overlap. As a result, there is a justified reason for conservative design that avoids all failure modes, though this approach may mask signs of weakening, and result in more extensive failure when preventative maintenance is neglected [7]. Instead, structures that have more than one defining characteristic and can experience multimodal failure may be analyzed with more than one numerical model, to ascertain the dominant failure mode by means of agreement between simulations [5] [10].

3.0 Methodology

3.1 Experimental Design

The purpose of the methodology section is to show the reasoning process behind the design of the experiment and to explain in detail the methods used to study the progression of damage in a multiple impact condition. In order to ensure their agreement, the computational model and experimental test need to be developed concurrently, such that the geometry, timescale, damage effects, and measurement methods are practical, in the physical and computational sense.

Based on a review of existing experimental methods, as given in section 2.3, a scale of 500 mm to 1500 mm was proposed for the experimental tests. Due to safety concerns regarding the shattering or rebound of the projectile, a lighter projectile was considered favorable. Finally, as both the projectile and slab required a fine mesh during simulation, the lower bound of which was determined by the aggregate size, the scale of the simulation needed to be such that the element count rendered the computational problem tractable. These considerations may be called the constraints of the research problem, and are summarized in Table 3.1. It can be seen from the table that there are inherent tradeoffs in the design variables – a smaller simulation scale is computationally efficient but detrimental to experimental error; a lower projectile speed increases the anticipated number of tests until failure is achieved.

Table 3.1 – Constraints of the research problem. Dimensions are given as characteristic lengths.

Constraint	Range	Objective	Justification
1. Slab dimensions	500 – 1500 mm	Low = better	Economy
2. Simulation scale	10 – 1000 k elements	Low = better	Economy
3. Projectile mass	1 – 10 kg	Low = better	Safety
4. Projectile velocity	10 – 50 m/s	Low = better	Safety
5. Projectile diameter	10 – 1000 mm	High = better	Accuracy
6. Meas. resolution	100 – 100,000 Hz	High = better	Accuracy
7. Desired damage depth	0 – 1 (Normalized)	High = better	Fewer tests

Given enough studies where experiment and simulation are studied together using the same testing methods and software, the solution to these constraints may be solved for by optimization methods. However, the literature review showed low consistency of choice of experimental and simulation methods among authors. The strategy for approaching the design of the four experimental components (air cannon, slab, projectile, reinforcement bracket) and their corresponding simulation counterparts was therefore as follows:

- First, a well-documented and relevant impact test was chosen from the literature, and modeled in LS-DYNA. The resulting simulation could be studied to determine the accuracy and efficiency of the LS-DYNA simulation environment. Various design choices could be tried out and studied, such as the type of concrete material model, timescale, mesh sizing, numerical convergence or instability, and formulation of boundary conditions. This process is presented in Section 3.2.1, Preliminary work.
- Once the material model, mesh, geometry, and boundary conditions are decided on, a sensitivity analysis of the specific model could be carried out with respect to initial conditions such as impact velocity and to internal parameters such as erosion and failure criteria. These results, documented in Section 3.2.1, extend the simulation behavior past the reference experimental test, and give a thorough understanding of the model behavior in trivial or extreme loading conditions. Additionally, these tests enable the tweaking of any global solver settings, such as minimum time step or damping controls.
- Now that a reference experimental test is modeled by a simulation, an estimate of the modified geometry and initial conditions is calculated. This effectively scales the design variables to find a viable solution for defining the research problem. For instance, the reference test chosen was the NSSA impact test, and the resulting damage zone was

shown to be proportional to the projectile frontal area. From this information a ratio of projectile size to slab size was selected, and scaled to minimize constraints 1, 3 and 5 in Table 3.1. Slab thickness was then scaled down to allow significant damage, with the corresponding adjustment to the measurement resolution.

- Finding a set of feasible problem constraints allows for the research problem to be simulated. To conduct the experiment, however, the design of the constraining bracket and air cannon is necessary. A separate design process is carried out for these assemblies in the classical manner, using the physical dimensions of the slab and projectile, as well as the initial velocity, as inputs. As long as the resulting design is not unreasonably expensive or impractical, it may be selected without further revision.

In practice, this process was carried out over an iterative fashion over the course of some 8 months, and in conjunction with the acquisition of some of the measurement equipment. The final values of the design variables are shown in the last column of Table 3.2. The first variables to be decided on were the slab dimensions and thickness (not shown), and the last variables to be tuned were projectile velocity and mass. The following sections will describe the specific reasoning behind these values, and cover the methods of acquiring and processing data.

Table 3.2. Reference and final values of the design variables.

Constraint	Range	Reference Value	Final Value
1. Slab dimensions	500 – 1500 mm	1200 mm	600 mm
2. Simulation scale	10 – 1000 k elements	5 k elements	48 k elements
3. Projectile mass	1 – 10 kg	6.8 kg	2.0 kg
4. Projectile velocity	10 – 50 m/s	45 m/s	20 – 25 m/s
5. Projectile dimension	10 – 1000 mm	150 mm	150 mm
6. Meas. resolution	100 – 100,000 Hz	1,000 Hz	7,000 Hz
7. Desired damage depth	0 – 1 (Normalized)	0.05 – 0.10	0.2 - 0.5 (est.)

3.2 Simulation Methodology

3.2.1 Preliminary work.

The National Storm Shelter Association (NSSA) Frontal Impact Test was selected as the reference test for this research paper, due to its well-documented setup and its use in providing certification for storm protection [2]. The test specifies that a 4x4 foot section of protective material impacted by a 15 lb wood stud is rated for a type of severe storm if it can prevent the perforation of the projectile accelerated to the corresponding rated speed. In the case of an EF-5 tornado, for example, the rated wind speed is in excess of 300 mph, and the rated projectile speed is 100 mph for horizontal surfaces [3]. The successful simulation of the test was the first significant milestone in the characterization of concrete impact dynamics. See Figure 3.1 for a visual of the simulation.

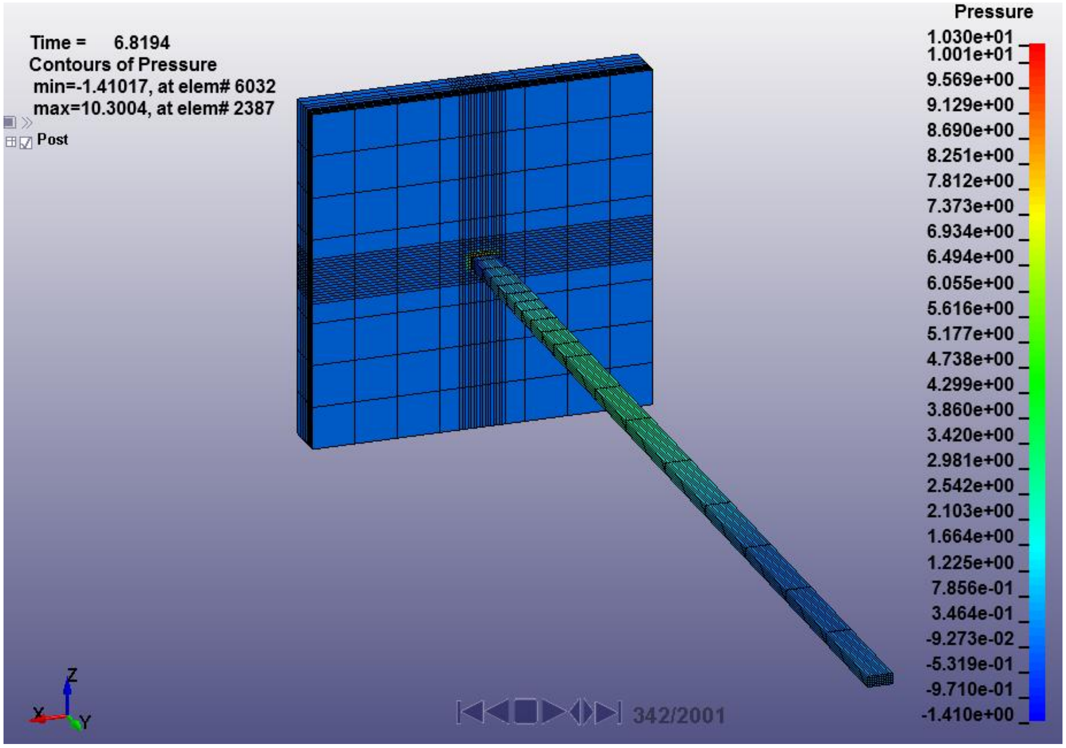

Figure 3.1. Simulation screenshot showing the impacting of a wood missile into a reinforced concrete slab.

The figure shows a pressure shock wave propagating through the wood stud at the time of 6.82 ms, after the wood rebounded. A zone of residual strain and compaction can be seen in a cross-section of the concrete, depicted in Figure 3.2. The residual plastic strain extends several millimeters into the surface, and has a high value (0.25), indicative of softer, compacted concrete or masonry. No damage extends to the back of the slab. This is consistent with the type of compaction that may be seen in low-strength residential-grade concretes, although this type of damage would be unacceptable in protective structures, where strain should not exceed 0.01.

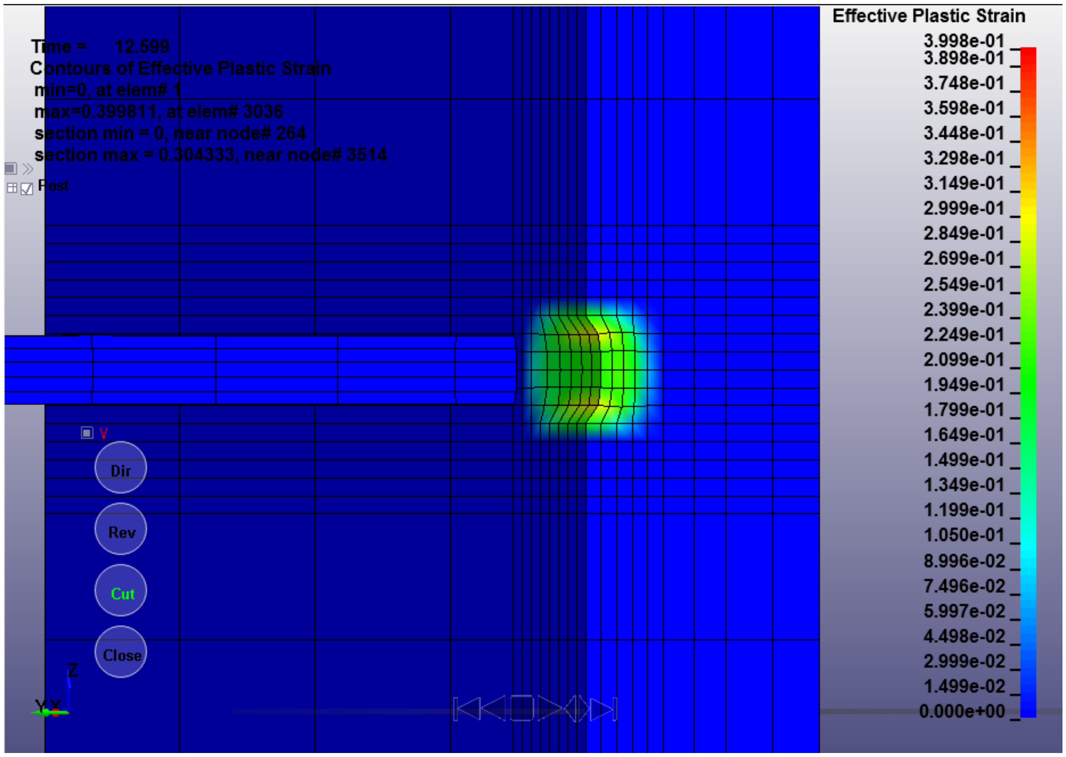

```
Time =      12.599
Contours of Effective Plastic Strain
 min=0, at elem# 1
 max=0.399811, at elem# 3036
 section min = 0, near node# 264
 section max = 0.304333, near node# 3514
```

Figure 3.2. Effective plastic strain remaining after impact.

Besides visual results obtained from the simulation, the nodal displacements and accelerations of the concrete slab were tracked at the centers of the front and back face. These provided helpful information on the type of acceleration data that may be collected by a center-mounted accelerometer in a physical test, and the type of displacements a slab may experience. Figure 3.3 shows a time history of the accelerations of the front and back nodes over the first two milliseconds. These results gave insight into the duration of impact and the time step resolution needed to accurately track variables. The figure also shows how the plastic deformation of the concrete material in the front causes a dilation of the vibrational response frequency.

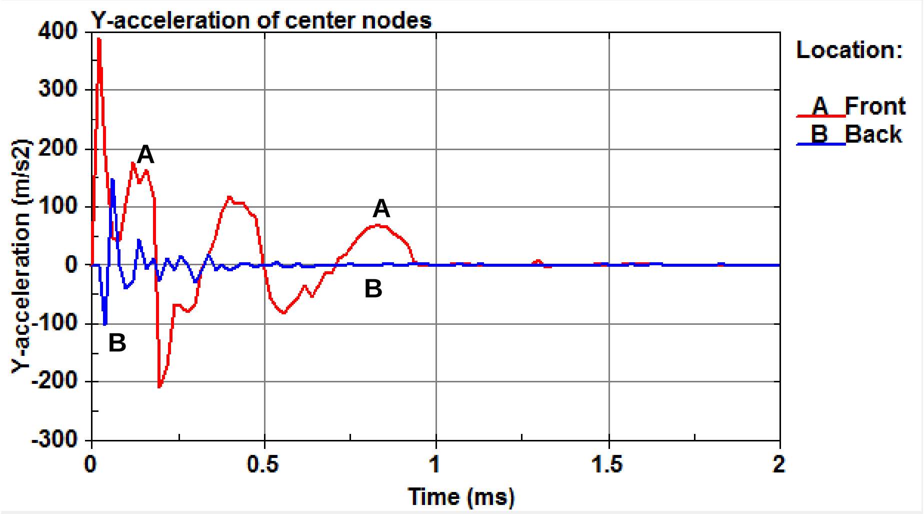

Figure 3.3. Acceleration nodal histories for the preliminary impact simulation.

A damage variable in the RHT concrete model allowed the assessment of compound damage, and the depth and area of the damage zone were found to be roughly half and twice the missile diameter, respectively [24]. In the case of a compaction failure, the damage was confined to the zone of plastic strain, and the damage visualization is essentially the same as that in Figure 3.2.

The initial simulation was optimized to run in a matter of minutes, to allow for easy troubleshooting. Mesh elements not in the immediate zone of impact were left very coarse, leaving the majority of the elements near the contact region. The model consisted of roughly 6200 elements, with element sizes ranging from 150 mm to 10 mm. Following these promising results, additional simulations of different sizes and qualities of mesh were performed. The results showed fair agreement with the initial effort.

Further useful insights were obtained from varying material parameters, as well as environmental variables. For instance, temperature and moisture effects were considered in the design of impact tests. The differences in nodal displacements for each scenario are summarized in Figure 3.4. The penetration depth difference was observable, but not significant.

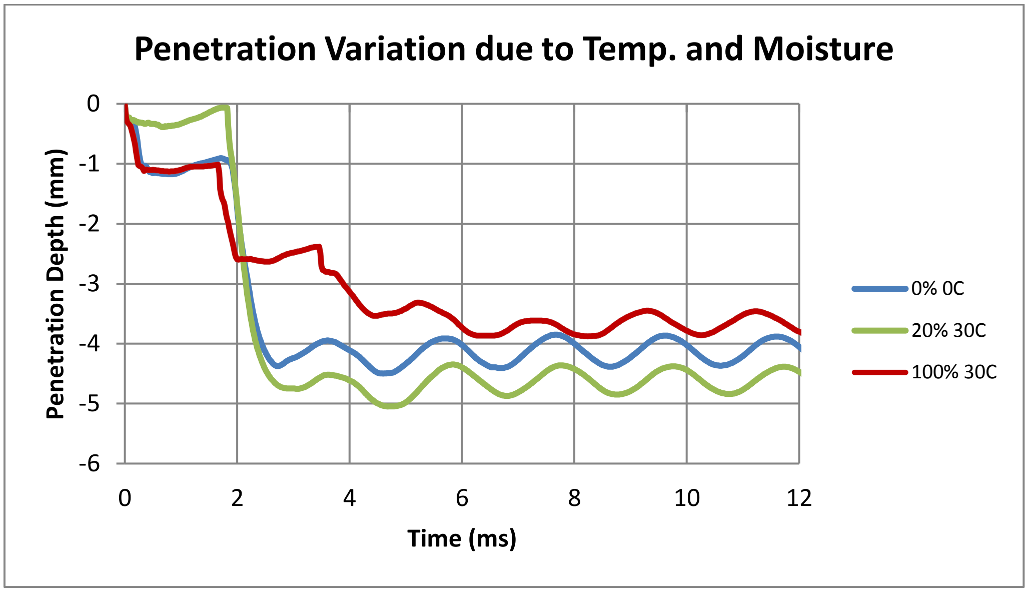

Figure 3.4. Penetration depth at various simulated environmental conditions. Legend shows % MC and deg C.

Finally, the impact speed was varied over a wide range to obtain a speed-deflection characteristic curve. The simulation data of the CSCM and RHT concrete models was compared to the predictions given by the NDRC and Kar formulas, and were found to lie between them. Figure 3.5 shows the data obtained.

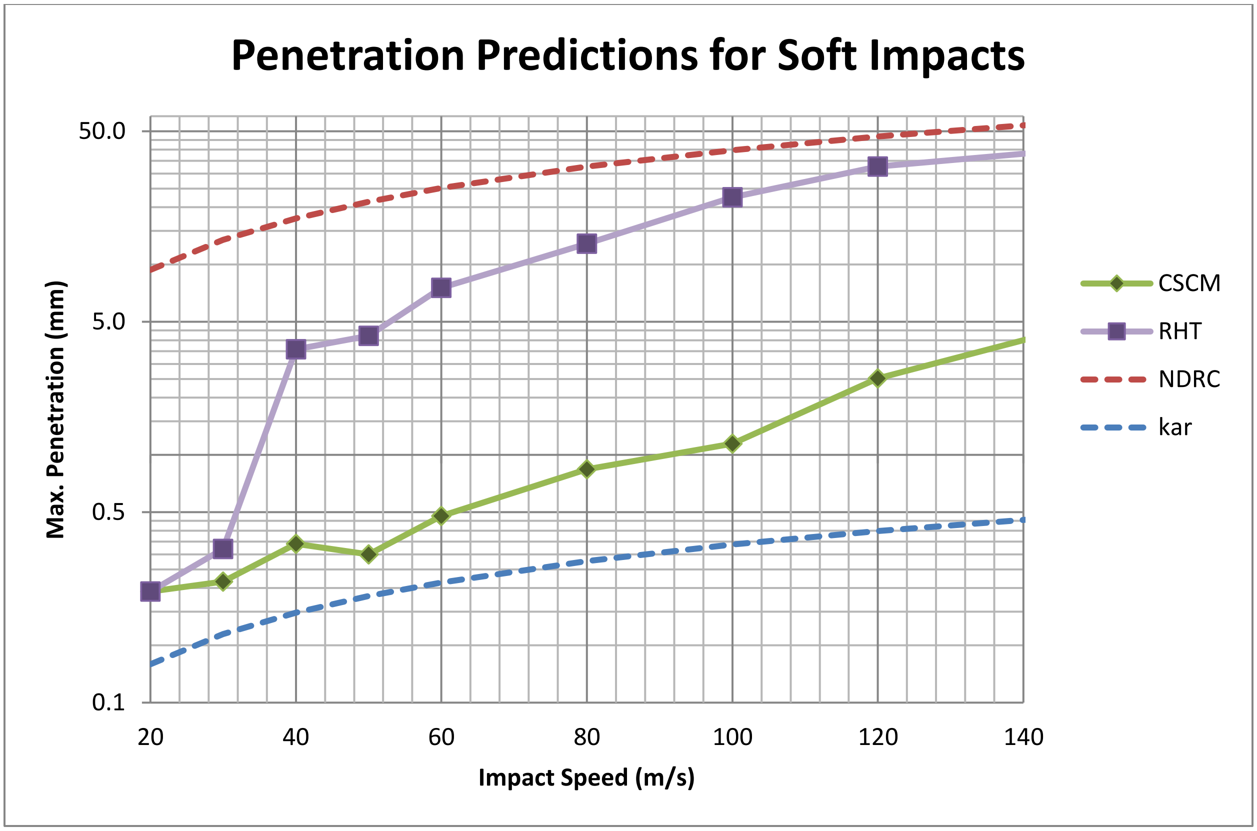

Figure 3.5. Velocity-dependent penetration predictions for soft missiles.

No tensile or plug failure occurred during the frontal impact test. To understand the difference in failure progression between concrete models, an unreinforced corner impact was modeled, as seen in Figure 3.6. The RHT and CSCM materials were compared, and erosion criteria were varied to determine the dependency of the dynamic behavior on the failure mode. Individual elements were found to display unrealistic strains after surpassing critical damage, however, the simulation displayed greater numerical stability and showed a comparable area of erosion with the RHT damage variable.

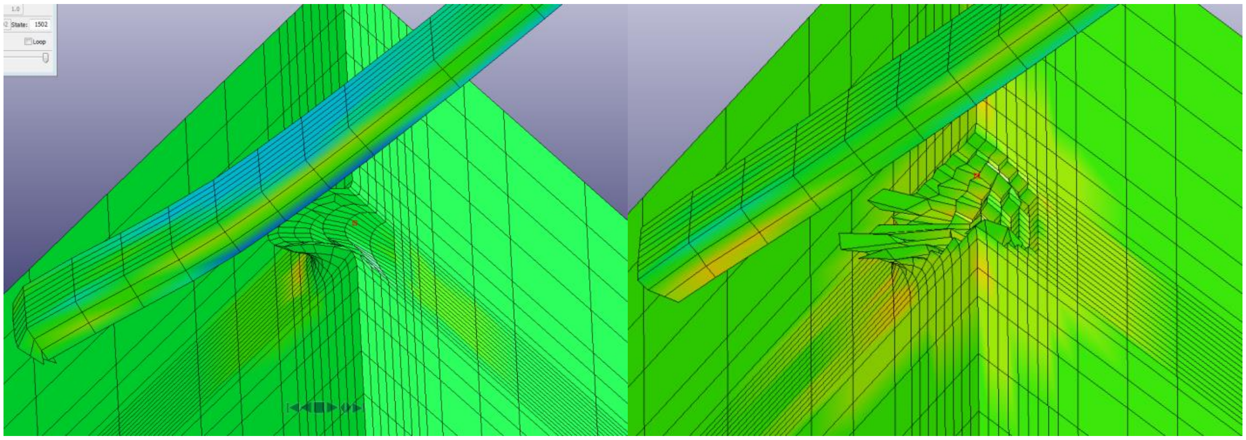

Figure 3.6. Corner impact test visualizations. RHT is on the left and CSCM is on the right.

Following the completion of these preliminary tests, the design variables for the final tests were finalized. The materials for the slab, projectile, and reinforcement were selected based on ease of use, numerical stability and intent of application.

3.2.2 Geometry

In order to accurately model the impact of a projectile into an RC slab, full-scale part geometries were created for the slab assembly (concrete and rebar) and the projectile assembly (wood stud and metal end-caps). The concrete was modeled as a 24x24x4 inch slab, and the rebar was modeled as 0.125 inch diameter wire spaced 6 inches apart to create a lattice. The rebar was positioned 1.0 inch from the back face of the slab. The solid models of the projectile, target slab and rebar were generated in Solidworks and exported to ANSYS. An illustration of the simulation model may be found in Figure 3.7. The model reflects the dimensions specified in the assembly drawings, which can be found in Appendix A.

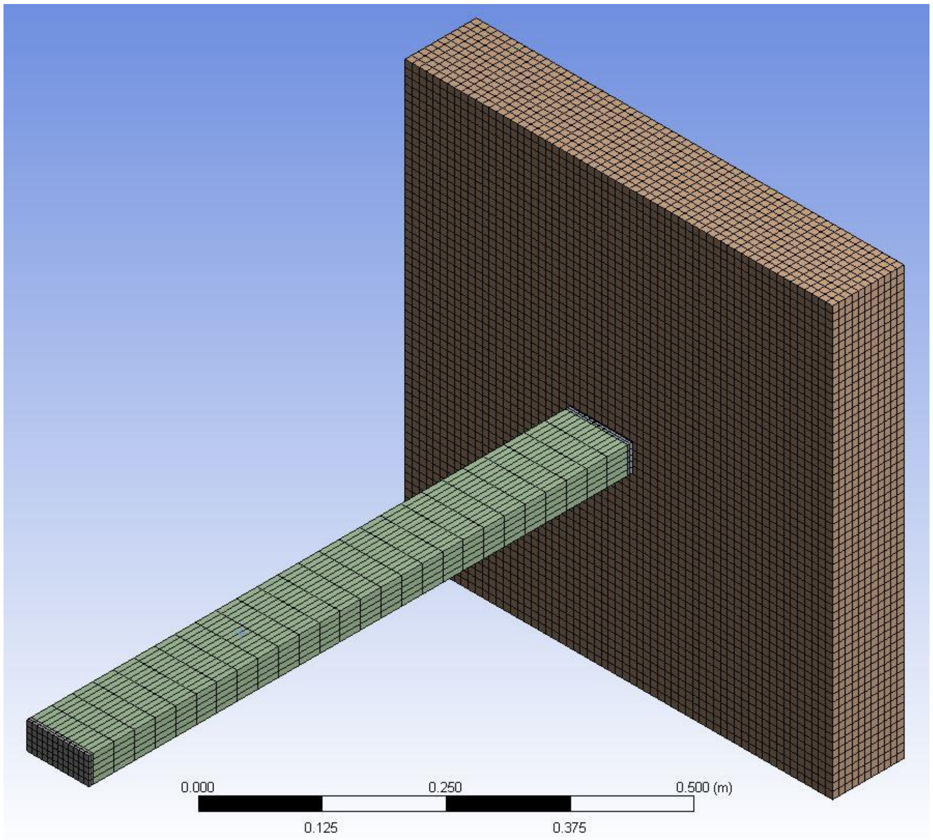

Figure 3.7. Illustration of the simulation model, showing the slab and composite projectile, as well as the element mesh.

3.2.3 Element and mesh

The projectile and target are discretized using default ANSYS 8-node hexahedral elements, which are then converted to a single point 8-node hexahedral element in LS-PrePost. These elements are simple and efficient, but possess zero-energy mode of deformation, where element nodes may move without the element experiencing average strain. A 3-node line element is used to mesh the rebar. Concrete element size was constrained to 10 mm to approximate the aggregate diameter. The projectile mesh was sized at 8 mm, to be comparable in scale to the slab mesh. The rebar, which was modeled as one-dimensional line elements, takes on a 20 mm element length. Figure 3.7 shows the meshes of the slab and projectile.

3.2.4 Material models

The materials used in the simulation are concrete, steel, and wood. Each material was assigned a model based on its anticipated behavior experimentally. Table 3.3 below summarized the material selection and full input parameters can be found in the LS-DYNA input deck in Appendix B. Default material properties, as determined by the developers of the material model, were selected unless otherwise noted in the table.

Table 3.3. Summary of material model selections.

Material	Role	Anticipated behavior	Material model	Controlled properties
Wood	Projectile	Nonlinear, Anisotropic	MAT_143 (USDOT)	Density
Concrete	Target slab	Nonlinear, Isotropic	MAT_272 (RHT)	Compressive strength
Steel	Caps, Rebar	Linear Elastic, Isotropic	MAT_003 (Elastic)	Density, Elastic mod.

3.2.5 Contact formulation

All projectile and slab element contacts were controlled by an automatic single contact algorithm, which and allows for penalty-based contact between any two penetrating elements. In this way, contact forces are applied from slab to projectile, but not between projectiles, so that a rebounding projectile would not interact with an incoming one in the multiple impact simulation. A special constraint formulation, “Constrained Lagrange in Solid” was used to relate the displacement and velocity of the nodes in the rebar to the nodes in the solid concrete element surrounding it. In this manner, the concrete elements containing the rebar will have the strength of steel as well as the concrete, while maintaining failure modes of both materials independently.

3.2.6 Timescale

The simulation time step is determined by the time interval a shockwave takes to travel through the smallest element. In this case, the steel components determine the size of the timestep, and LS-DYNA automatically makes an initial prediction from the element geometries. During the course of the simulation, the timestep may be reduced due to large element strains. Typically, simulations run with the geometry described above had a time step on the order of 1E-6s, giving a resolution of 1000 steps per millisecond. The system state is written to a database on a larger, user-specified timescale of 0.1 milliseconds. In addition, every 5000 time steps, runtime statistics are calculated, showing average computational time per cycle, ranging from 100 ms to a few seconds. In this manner, simulation stability can be tracked. The control parameters input into the simulation can be found in Appendix B.

3.2.7 Post-processing procedure

After the simulation has completed, a standard procedure is followed to verify accuracy and to obtain standardized, comparable results. Because of the explicit solver used, a review of part energies over the time history of the simulation is important to verify energy conservation and hence simulation accuracy. Additionally, tracking the hourglass energy for all reduced integration point elements ensures that deformations are due to physical strains and not zero-energy modes of the elements. Table 3.4 below summarizes the sequence of actions to process simulation results.

Table 3.4. Summary of post-processing steps.

P01	Run simulation and write files to LS-DYNA database.
P02	Load simulation files into LS-PREPOST.
P03	Check simulation stability over the timescale.
P04	Track the kinetic energy of the slab part to ensure proper energy dissipation.
P05	Track the nodal acceleration in the impact region to obtain the concrete's modal response.
P06	Identify the stresses and strains in the impact region.
P07	Identify the extent of damage using the damage variable.
P08	Export the deformed state of the elements for further simulation work.
P09	Export charts, figures and animations for publication.

3.3 Experimental Methodology

The experimental setup was designed primarily with the purpose of safety in mind. The air cannon, power equipment, user controls and trajectory alignment were positioned away from the impact to minimize health hazards. The slab was constrained in the reinforcing bracket and covered on the sides by a protective enclosure consisting of plywood and cinderblock. The enclosure prevented debris generated on impact from flying out of the designated impact zone.

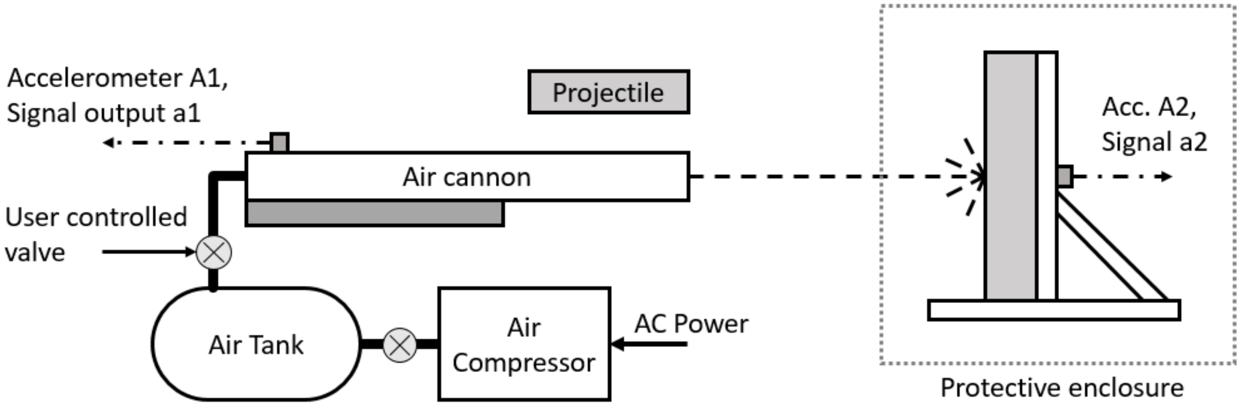

Figure 3.8. Schematic of test setup and equipment. The user activated a high-flow-rate valve between the air tank and barrel. Which triggered data collection from both accelerometers.

3.3.1 Projectile

The projectile consisted of a rectangular beam of spruce wood with two metal end caps, and was wrapped in duct tape to prevent splintering on impact. Projectile dimensions were 30” long and 1.5x3.5” in cross section, as detailed in Appendix A. Projectile masses were kept consistent to 1950g +/- 50g. Ten interchangeable projectiles were fabricated to allow for replacement mid-test. Projectiles were found to crack and buckle after a few impacts.

3.3.2 Concrete slab pour

The concrete slabs were created by mixing and pouring Quikrete 5000 industrial concrete mix according to manufacturer recommended instructions. One batch per slab was prepared using an industrial mixer. Reinforcement was positioned at the beginning of the pour, and consisted of

0.125 inch steel wire. Two test samples per slab were poured into 2x2x2 inch ASTM molds at the time of the pour, and allowed to cure in lab conditions alongside the concrete slab. Compressive tests were carried out on concrete samples after 4 weeks of curing. The test procedure is given by ASTM C109 [1]. The compressive strength was found to be 32.5 MPa, with a standard deviation of 1.6 MPa.

3.3.3 – Air cannon.

A dedicated air cannon was fabricated for testing, following the design of pneumatic projectile launch devices described in ASTM E1886 [2]. Refer to Appendix A for design dimensions. The air cannon was expected to operate at pressures as high as 690 kPa, and accelerate the projectile to speeds of 40 m/s. In practice, a more conservative speed of 20 m/s proved to be sufficient for creating a damaging impact.

3.3.4 - System Calibration.

Preliminary analysis and tests showed that a repeatable impact location was important for obtaining consistent vibrational response results. The slab was positioned 1.0 m away from the air cannon barrel to minimize free-flight time. The air cannon orientation was adjusted optically at the beginning of the test so that the projected impact location was within 5% of the geometric center of the slab (25 mm deviation). Subsequent projectile firings resulted in a high repeatability of within 2% of the initial impact location. Projectile speed varied due to friction and pressure release conditions, and was repeatable to within 10% of the mean value.

3.3.5 – Data acquisition.

Two accelerometers from PCB Piezotronics (Model 353B03) were selected to mount on the air cannon and the back face of the slab. The accelerometers collected data up to 300 g and 7000 Hz. The primary mode of vibration of the slab was predicted to be around 1 kHz. The accelerometers were triggered to begin data acquisition by the initial acceleration of the air cannon valve. Data for projectile impact was synchronously recorded for 3000 ms after the trigger was tripped.

A Quattro 4000 data acquisition switch from Data Physics collected and superimposed the signals at the rate of 7,000 data points per second. The signals were then processed on Data Physics spectral analysis software to give the time history and the power spectrum response. The time lag between acceleration peaks of the two signals was measured to calculate the average projectile speed. Figure 3.9 shows a schematic of the signal path.

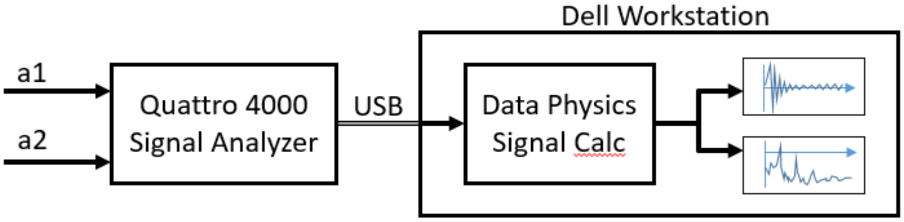

Figure 3.9. Schematic of the signal path. Signals were obtained in real-time and stored in a signal buffer. The spectral analysis was carried out after the signal was transferred to the Signal Calc software.

3.3.6 – Test procedure.

The experimental test was carried out by two operators in accordance to a written test procedure, shown in Table 3.5. Testing was carried out outside the lab due to risk of flying debris.

Table 3.5. Summary of testing steps. Refer to schematic in Figure 3.8 for labeled locations.

T01	Ensure release valve is closed. Pressurize the air tank to a reference pressure with the compressor.
T02	Load the projectile to a specified depth D1 into the barrel. Ensure clear flight path.
T03	Initialize accelerometers A1, A2 to begin data collection on trigger.
T04	Enclose the protective zone to prevent debris spalling. Verify all operators are in safe zones.
T05	Open operator-controlled valve to fire the projectile into the concrete slab.
T06	Collect and save the accelerometer signals a1 and a2. Calculate time of flight.
T07	Measure, photograph and mark the impact location of the projectile in the slab.
T08	Inspect the slab, projectile, and accelerometer mount for damage or delamination.
T09	Replace all components to initial locations if dislocation or damage occurred.
T10	Clean up any debris. Repeat steps for continued impacts. Terminate test when the slab forms a plug.

4.0 Results

4.1 Simulation Overview

The resultant simulation included 56707 nodes and 48203 elements, 85% of which formed a 61x61x11 element discretization of the concrete slab that defined the problem domain. Slab element dimensions were limited to 10.0 mm due to aggregate size. Projectile elements were slightly finer at 8.0 mm, both to preserve the coarseness of the wood grain and to allow for well-conditioned contact between slab and projectile elements. The mesh was highly regular, with all nodes in a part uniformly spaced.

Each simulation run completed in approximately 140 minutes, running on an Intel i7-4770 CPU at 3.4 GHz, with access to 16 GB of 1600 MHz DDR3 SDRAM. The simulation timestep varied between 5E-7 and 2E-7 seconds, with longer times required when processing failed elements. Overall, 87% of CPU resources were used for solid element processing, and 8.2% of resources were used for contact interactions, and 4.8% for data operations and program tasks. The simulation generated approximately 20 GB of data, with an output resolution of 0.0001 s over 0.0400 s. This resolution allowed for the computation of power spectrum responses up to a frequency of 10 kHz, comparable to the experimental signal obtained from the accelerometers.

4.2 Single Impact Results

4.2.1 Part energies and strain accumulation

In the first simulation set, a single impact between a projectile and a slab is studied. The simulated impact predicted a contact time between the projectile and slab of 0.650 ms, and a rebound velocity of 4.65 m/s. During that time period, 240 J and 42.5 J of energy are dissipated into the projectile and slab as internal strain energy respectively, as shown in Figure 4.1.

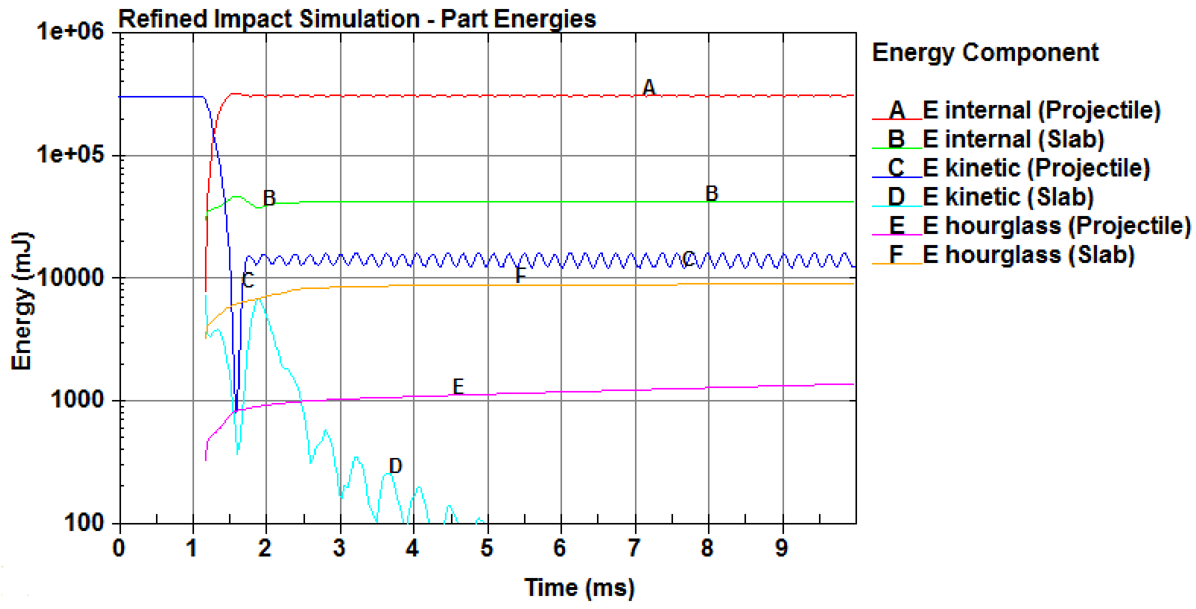

Figure 4.1. Energy component time histories of the slab and projectile. Internal energies represent elastic and plastic strain. Hourglass energies verify model stability.

The bulk of the energy transfer occurs between 1 and 2 milliseconds, when the kinetic energy of the projectile becomes transferred as internal energy to the slab and projectile. Lines A and B show the plastic strain of the two bodies level off to a steady state, although some oscillation continues in the projectile. The kinetic energy of the projectile (line C) briefly goes to near-zero, and then increases to a steady state value, corresponding to the rebound velocity. Due to an undamped elastic shockwave traveling through the material, the projectile velocity is not constant. The concrete, on the other hand, is constrained and damped, so that the kinetic energy, shown by line D, asymptotically approaches zero. The hourglass energies of the slab and projectile (line E and F) are also tracked to verify that energy is distributed evenly within an element locus. Hourglass deformation is a type of element deformation that produces trapezoid-like displacements while keeping the element strain and volume the same. To ensure that the displacements are accurate and not due to the excitation of this deformation mode, hourglass energy can be monitored and controlled by LS-DYNA. The positive slope of the projectile hourglass energy, represents an increase of element hourglassing in the projectile, eventually leading to local instabilities. For the purposes of this work, the hourglass energy is only of concern if it reaches a relatively high value (> 5% of total energy) during the impact itself.

The damage to elements deformed under plastic strain are visualized in Figure 4.2 using the RHT damage variable (written to history variable #4 by LS-DYNA). This damage value is computed from the accumulation of plastic strain, and corresponds to zones where shear and tensile cracking may occur. From the visual it is estimated that a volume of 153 cm^3 developed significant (D > 0.20) damage [7].

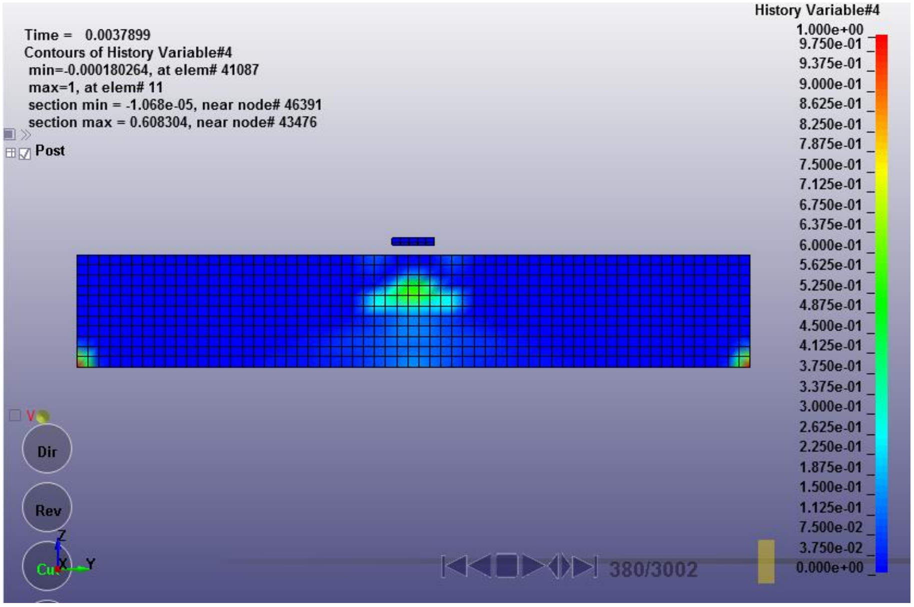

```
Time =   0.0037899
Contours of History Variable#4
 min=-0.000180264, at elem# 41087
 max=1, at elem# 11
 section min = -1.068e-05, near node# 46391
 section max = 0.608304, near node# 43476
```

Figure 4.2. Cross section of the slab after impact, showing concrete damage below the impacted surface. Damage concentrations are also present at the slab corners, where the boundary conditions were applied.

Figure 4.2 shows that the bulk of damage occurs in the subsurface region where shear stresses are dominant. This finding is significant because it represents high damage values (D > 0.4) that may not be visible after a physical impact, but may still weaken the concrete. Additionally, damage concentrations develop along the edges of the slab, which is expected in constrained nodes on the free surfaces of brittle materials. Although there are no significant consequences of these localized failures, careful attention must be paid to the boundary region, to ensure that no damage effects are caused by the imposed boundary conditions.

4.2.2 Slab stresses and strains

Pressures, strains and shear stresses are tracked throughout the domain to determine the heaviest contributors to resulting damage. Tensile strain in the back face of the slab and shear stresses in the subsurface region along the perimeter of the impact zone are found to be significant enough to cause the development of growing damage zones. Zones of pressure exceeding the compressive strength of the concrete developed directly under the projectile contact area, eventually causing surface compaction. A comparison of shear stress, plastic strain and pressure fringes is shown in Figure 4.3, with clear similarities visible in the shape and extent of zones of localized stress and strain.

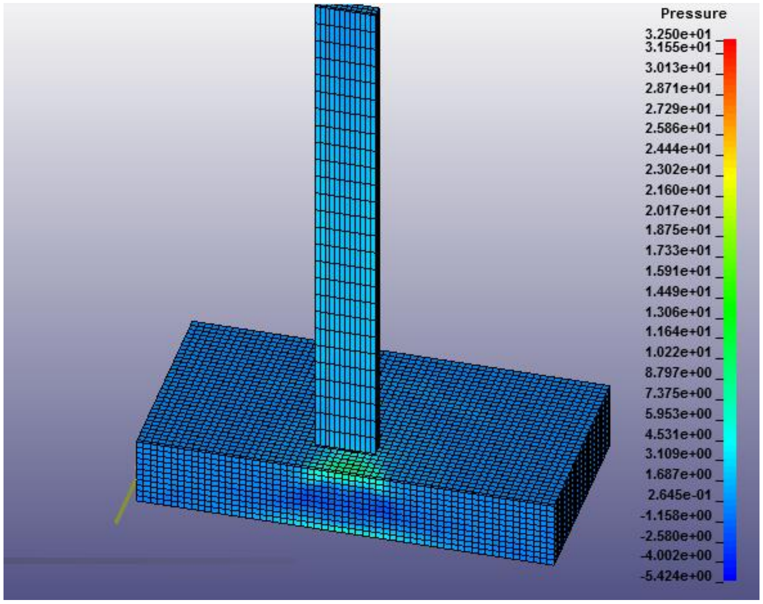

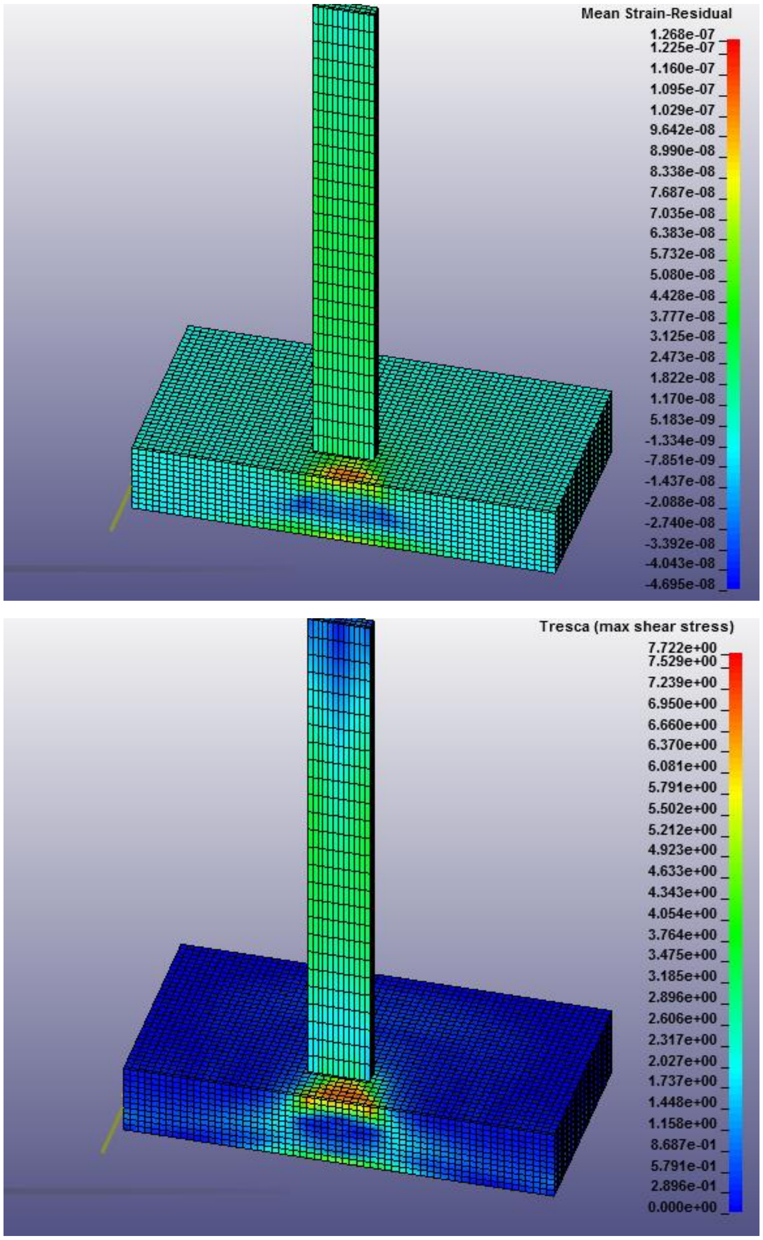

Figure 4.3. Visual comparison of Pressure (top), residual mean strain (middle) and residual shear stress (bottom). A shear failure mode will result in the formation of a tapered plug separating from the slab. The shape of the developing plug can be seen above.

The impact is considered to end at 10.0 ms. At this time, Figure 4.3 A shows residual pressures of 15 MPa in the compressive region and -5.4 MPa in the tensile region. Residual mean strain is 1.2 E-7 (compressive) and -0.4 E-7 (tensile), as shown in Figure 4.3 B. Residual shear stress is highest on the impact surface: 7.7 MPa.

4.2.3 Nodal displacements and accelerations

The complete simulated response of the slab allowed a time signal to be extracted from the nodes in the back face of the slab, effectively simulating the signal picked up by an accelerometer placed at those nodes. The displacement and acceleration of the slab is shown in Figure 4.4. The acceleration signal shows a peak of 30,000 m/s^2, which is in excess of the range of inputs recordable by the physical accelerometer. Additionally, the simulation predicts a dynamic deflection of 0.172 mm.

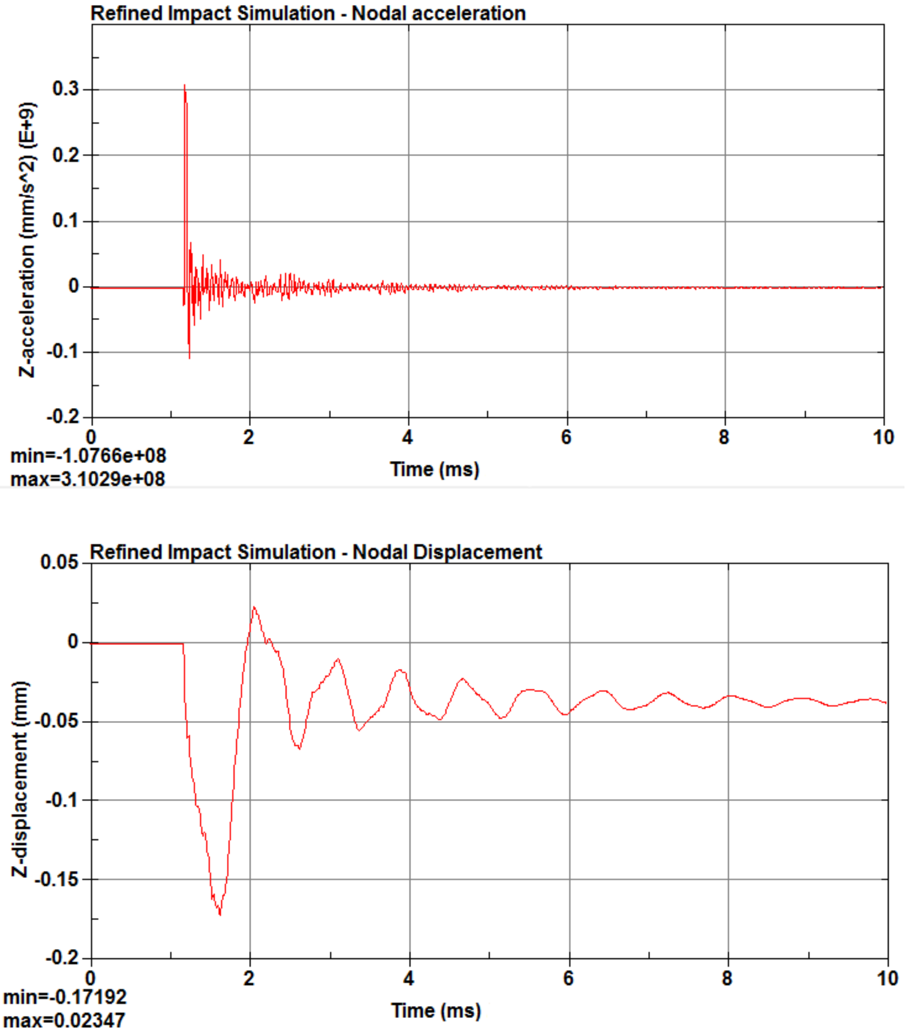

Figure 4.4 – Time history of acceleration (top) and displacement (bottom). Four nodes surrounding the center of the slab were selected and averaged to represent the readings picked up by a mounted accelerometer.

4.2.4 Damage verification

A comparison of the observed damage and strain data with an equivalent concrete model, MAT 159 CSCM Concrete, shows that the plastic strain region was of a consistent size and shape, with similar energy dissipation. This step ensures that the damage observed with the RHT model was interpreted correctly, and was independent of model-specific strain-based failure parameters which are not accounted for in the methodology section. A figure comparison is not shown due to the similarity of results.

4.3 Multiple Progressive Impact Results

Significant damage is observed after the first impact, and three additional projectile impacts are performed at regular intervals on the damaged slab. Damage formation begins as subsurface compaction and shear plastic strain and continues to accumulate during subsequent impacts, developing a plug-like region of damage similar to that from an explosive charge [9]. In addition to the internal damage, crack-like patterns begin to emerge and propagate along the back face of the slab. The detailed results are described below in the same format as the single impact.

4.3.1 Slab energies

Overall, the slab experiences a buildup of internal energy while the kinetic energy is dissipated, as shown in Figure 4.5. Less strain energy is accumulated in successive impacts as compared to the initial impact; projectiles have higher rebound velocities as a result of this.

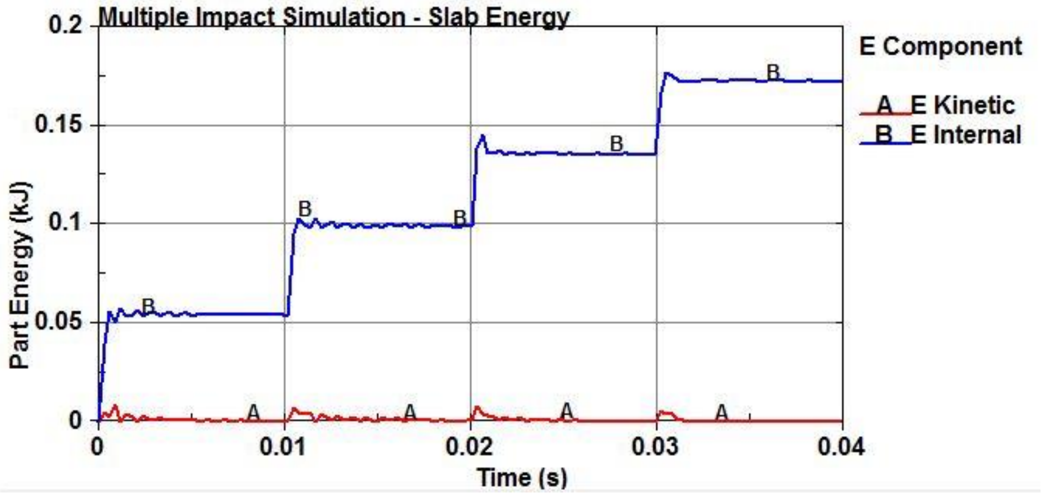

Figure 4.5. Component energies of the Slab showing accumulation of internal energy over successive impacts.

4.3.2 Strain and damage accumulation

The accumulating internal energy results in a larger zone of damage, which is illustrated in Figure 4.6 below. With the second impact and onwards, the conical shape of the plug becomes more apparent. It is also noteworthy that no progression of damage occurs at the edge boundaries, corresponding to a “settling in” of the slab into its fixture.

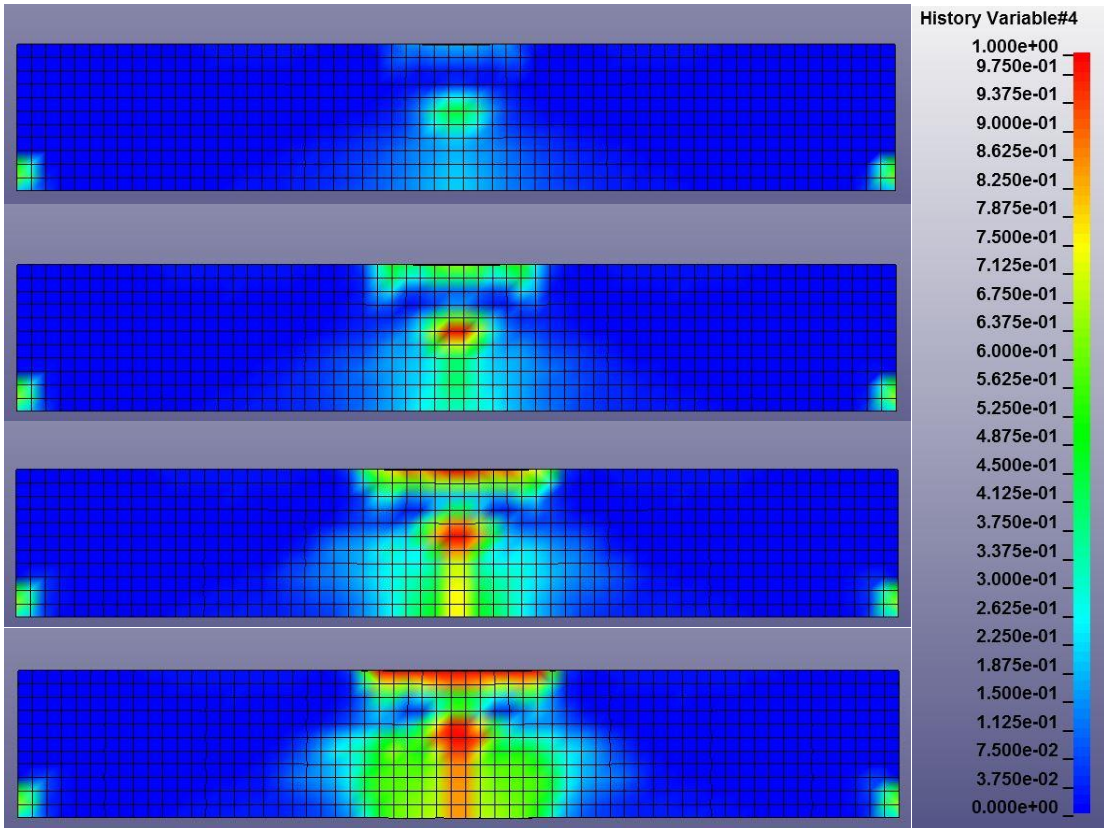

Figure 4.6. Visualization of the RHT damage variable over 4 impacts. A section along the plane of symmetry allows observation of internal damage.

In conjunction with internal damage, surface damage due to tensile strain accumulates on the back face of the slab. Figure 4.7 shows the developed radial crack regions after the final impact, displaying four-fold symmetry. This is consistent with the experimental results seen in the literature review, where crack patterns form radially around a plug.

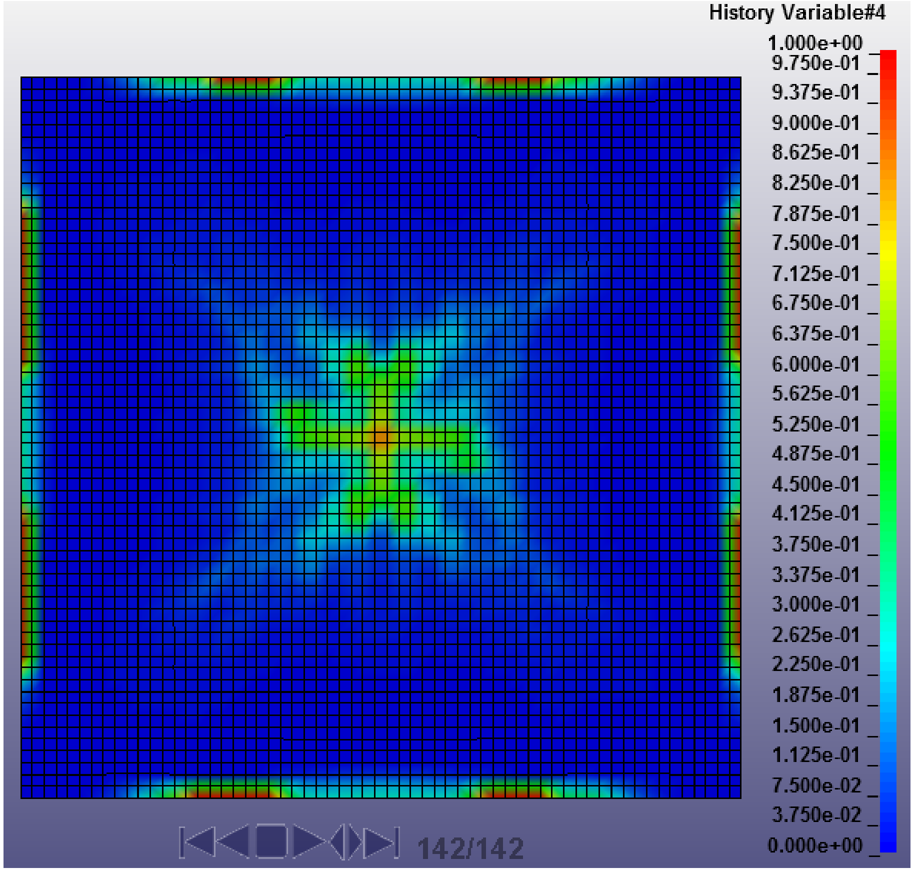

Figure 4.7. Back face of the slab, showing 4 crack regions emanating way from the crack nucleation site in the center.

4.4 Experimental Results

4.2.1 Concrete strength and properties

After the completed pour and curing period, the concrete slabs are tested to measure mechanical properties. Compressive strength is measured using the ASTM sample cubes set aside from the original pour. The maximum aggregate size was found to be 10.0 mm, and density after curing was calculated to be 2310 kg/m^3. These measurements were correlated to the parameters of the numerical material model. Table 4.1 shows the test data for the concrete samples.

Table 4.1. Compressive strength test data for two ASTM sample cubes.

Sample	Length [in]	Width [in]	Height [in]	Top area [in^2]	Fail load [lbs]	Strength [psi]
3.1	1.98	1.92	1.98	3.792	17000	4480
3.2	1.99	1.95	1.99	3.881	19300	4970

4.2.2 Air cannon tests

Five preliminary calibration and verification tests were completed with the air cannon using slab #1. These tests had a high variability of impact location and the data was not incuded in the analysis. Five impact tests are then performed with calibrated projectiles on slabs #2 and #3. Table 4.2 shows the recorded impact test data. Additionally, photographic data is taken directly following each impact. The trajectory deviation of each projectile is defined as the distance from the center point of its footprint to the geometrical center of the slab. This is done to verify that the impacts occurred approximately in the center of the slab. Figure 4.8 shows an example of the raw and marked up photographs of the tested slabs.

Table 4.2. Recorded impact test data.

Impact	Projectile	Mass [kg]	Press.[psi]	Dist.[m]	V_{AVG}[m/s]	Observed damage
2.1	1	1.964	80	3.21	24.1	4 radial cracks front/back
2.2	2	1.555	80	3.39	25.4	Plug outline, multiple spall pts.
3.1	3	1.994	60	3.20	20.2	4 radial cracks back
3.2	3	1.994	60	3.20	18.6	3 radial cracks front
3.3	4	1.901	60	3.21	24.8	Fracture, spalling

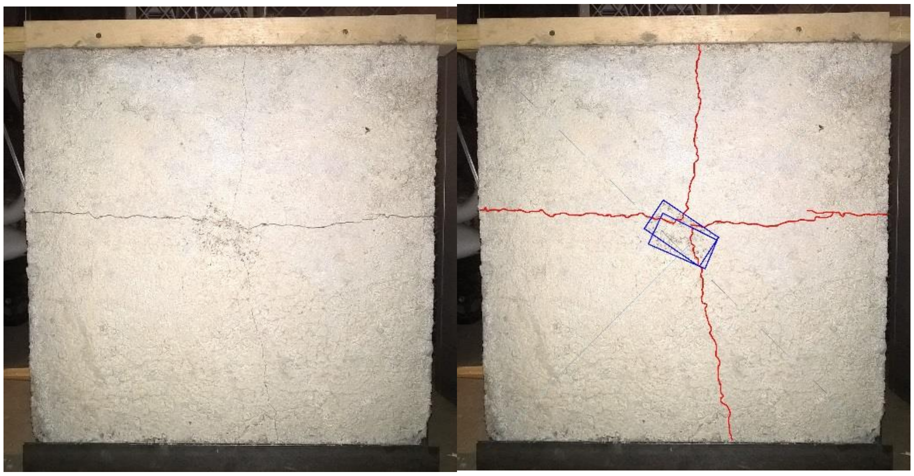

Figure 4.8. Raw (left) and processed (right) images of an impacted slab. The overlaid rectangles correspond to identified footprints of projectiles, and show significant overlap.

4.2.3 Accelerometer data

Accelerometer readings are recorded over a 3.000 s period following the initial trigger, with each accelerometer having a separate channel linked to the same time series. The overlay of signals allows for the computation of the time interval between launch and impact, which in turn enables the average velocity of the projectile to be found in Table 4.2. Figure 4.9 shows a time series signal of two accelerometer channels, and the corresponding power spectrum response.

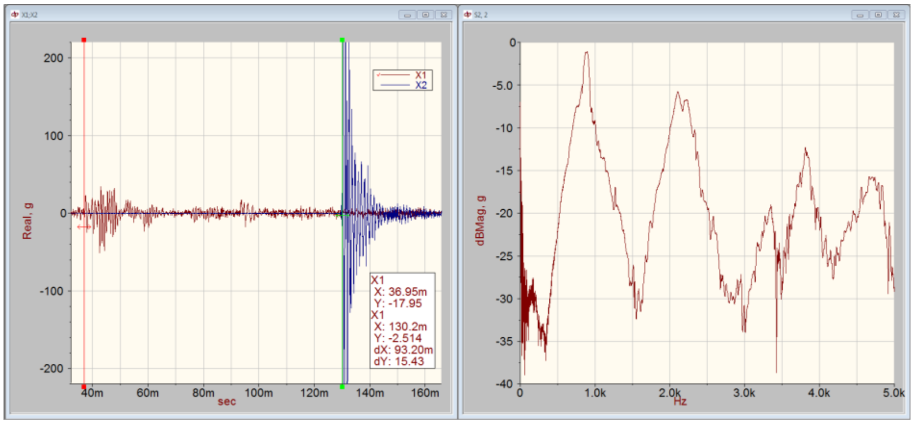

Figure 4.9. Accelerometer data from an experimental test (left) and the corresponding power spectrum response (right).

The slab accelerometer signal is cropped and analyzed for a modal and power spectrum response, with mixed success. Some power spectrum data is collected, but in some of the tests the pressure shockwave caused the accelerometer to detach from the back surface of the slab, devaluing the data immediately after impact. Figure 4.9 shows a well-conditioned power spectrum response.

4.2.4 Failure modes

Several modes of failure have been previously identified for concrete slabs. Below, Figure 4.10 shows experimental evidence for three of the modes: tensile cracking, plug formation, and surface spalling. These modes appear to develop concurrently in a test specimen, with each failure mode intensifying the development of the other two. Specifically, spalling effects are exacerbated by the creation of free surfaces that form as a result of deep crack propagation, while plug formation weakens the shear strength of the slab, allowing faster tensile crack propagation.

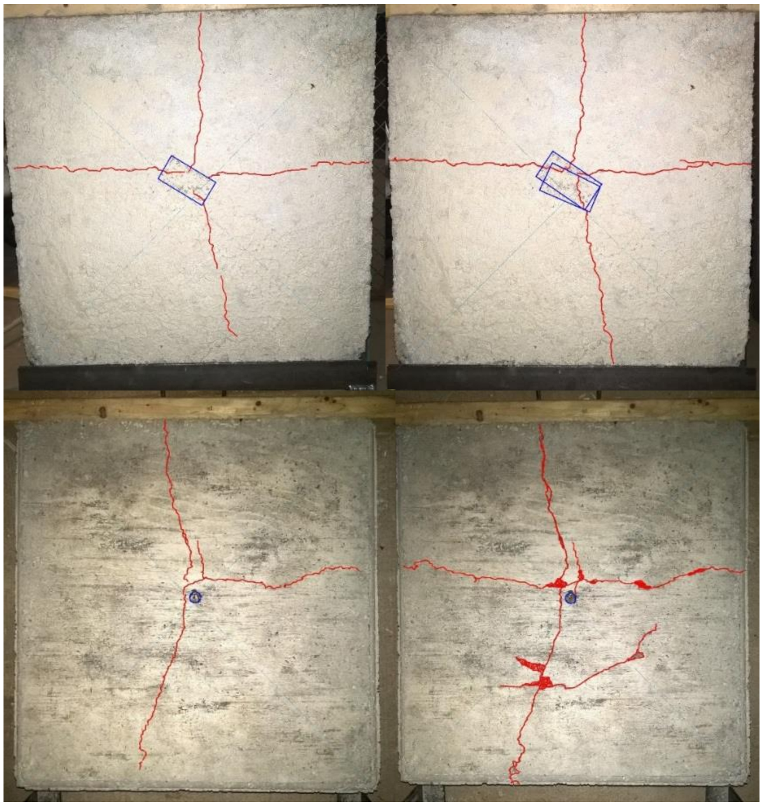

Figure 4.10. The front (top) and back (bottom) faces of the slab after impacts. Images on the left show impact 1, images on the right show impact 2. Formed cracks and areas of spalling are shown in red. Accelerometer location and wood projectile location are shown in blue.

To confirm the plug failure mode, which was expected to initiate in the interior of the slab, a section cut is taken with a concrete saw. In Figure 4.11, the cut-out material shows that the plug fracture line is indeed conical. The center of the cone contains a cavity where the concrete was pulverized during impact. This is consistent with the zone of highest stress and damage as seen in the simulation.

Figure 4.11. The cross section of the impact zone, showing a plug-like conical cracking pattern along the bottom of the sample. The cavity can be seen in the center of the sectioned block.

5.0 Conclusions and Future Work

The purpose of the work at hand was to predict, observe and verify the effect of impact loads in a multiple impact condition. To that extent, the numerical simulations and experimental results provided evidence that noncritical impact loads, when compounded, can and do induce multiple failure modes in concrete. Damage zones that initiated as barely observable cracks developed into zones of macroscopic cracking and plug formation over the span of a few impacts. This is the first work to document failures between singular fractures and low-cycle fatigue failures in a quantitative way.

In many respects the level of agreement of the experimental results and numerical predictions was higher than expected. Both the experiment and the simulation showed the combined failure effects of plug formation and tensile crack propagation. The best justification for this observation is the sophisticated formulation of the numerical models, which have been improving steadily in quality and performance over the last decades. In turn, it is possible to use the numerical model of the problem to predict the behavior of structures with enough detail to observe specific modes of failure. Still, differences between experiment and simulation remain. The coupling of the simulation to an experimental test allowed observation of subtle effects such as the orientation of the radial cracking pattern on the back face. Subsequent analysis of this phenomenon tied back to work in boundary conditions of classical solid mechanics, and suggests that these considerations remain relevant in problems of explicit dynamics.

Further work remains to be done in this line of research if the results are to be well understood and extended to practical problems of commercial design. Primarily, repeated testing of the multiple impact condition with a variety of projectile velocities, geometries and densities will generate an important data set bridging the knowledge bases of low-cycle fatigue with singular brittle fractures. This may include multi-material projectiles such as vehicles or complex projectiles such as living trees. In addition to observing the damage progression of structures, it would be useful to correlate the effects of a single high-velocity impact to series of impacts that impart an equivalent cumulative strain energy. This work would be of practical importance in determining the effective impact load that a structure must be designed to bear in order for it to withstand a given number of lesser loads distributed over its lifespan. This type of design method may be applied to military protective barriers, saferooms, structural transportation infrastructure, and may be incorporated into construction codes for long-lifespan projects.

As a final note, it is important to consider that the effects of scale were not captured in much of the literature review and the experimental and simulation work itself. Because the effects of cracking and failure are especially important in large-scale, singular projects, the observed phenomena in this work should be extended and tested against a variety of scenarios on a number of scales before broad design generalizations are drawn.

6.0 References

[1] ASTM C109/C109M-16a. Standard Test Method for Compressive Strength of Hydraulic Cement Mortars (Using 2-in. or [50-mm] Cube Specimens), ASTM International, West Conshohocken, PA, 2016.

[2] ASTM E1886-13a. Standard Test Method for Performance of Exterior Windows, Curtain Walls, Doors, and Impact Protective Systems Impacted by Missile(s) and Exposed to Cyclic Pressure Differentials, ASTM International, West Conshohocken, PA, 2013.

[3] "ICC/NSSA Standard for the Design and Construction of Storm Shelters," 2008 (ICC 500). International Code Council.

[4] "LS-DYNA Keyword User's Manual," R7.1 ed: Livermore Software Technology Corporation, 2014.

[5] A. Abu-Odeh, "Modeling and Simulation of Bogie Impacts on Concrete Bridge Rails using LS-DYNA," in 10th international LS-DYNA Users Conference, Livermore Software Technology Corporations, June, 2008, pp. 8-10.

[6] A. Amirikian, "Design of Protective Structures (A New Concept of Structural Behavior)," NP-3726; NavDocks P-51 United States, 1950.

[7] R. G. Bea, "Preliminary Root Causes Analysis of Failures of the Oroville Dam Gated Spillway," University of California Berkeley, Center for Catastrophic Risk Management, 2017.

[8] D. J. Benson, "The history of LS-DYNA," ed: Livermore Software Technology Corp., 2006.

[9] T. Borrvall and W. Riedel, "The RHT Concrete Model in LS-DYNA," LS-DYNA Users Conference, 2011.

[10] R. M. Brannon and S. Leelavanichkul, "Survey of Four Damage Models for Concrete." Sandia National Laboratories, 2009.

[11] Y. Chen and I. M. May, "Reinforced Concrete Members Under Drop-Weight Impacts," Proceedings for the Institution of Civil Engineers, 2009, pp. 45-56.

[12] W. L. Coulbourne, E. S. Tezak, and T. P. McAllister, "Design guidelines for community shelters for extreme wind events," Journal of Architectural engineering, vol. 8, pp. 69-77, 2002.

[13] M. Fakhari, B. Linderman, J. Rotz, and M. Suarez, "Design of Structures for Missile Impact," Bechtel Corp., San Francisco, California, 1972.

[14] A. F. Fossum, and R. M. Brannon, "The Sandia geomodel: theory and user’s guide," Sandia National Laboratories, 2004.

[15] J. O. Hallquist, "Preliminary user's manuals for DYNA3D and DYNAP (nonlinear dynamic analysis of solids in three dimensions)," UCID-17268 United States, 1976.

[16] R. J. James, L. Zhang, and J. Y. R. Rashid, "Impact of High Velocity Objects Into Concrete Structures - Methodology and Application," ASME, 2003.

[17] A. K. Kar, "Impact Load for Tornado-Generated Missiles," Nuclear Engineering and Design, vol. 47, pp. 107-114 1978.

[18] R. P. Kennedy, "A Review of Procedures for the Analysis and Design of Concrete Structures to Resist Missile Impact Effects," Nuclear Engineering and Design vol. 37, pp. 183-203, 1976.

[19] K. E. Kurrer, The history of the theory of structures: from arch analysis to computational mechanics. John Wiley & Sons, 2012.

[20] C. Moore, B. Kimball, M. Weaver, M. Barton, R. Phatak, and B. Conway, "Experimentation and Structural Analysis of OZ Saferooms," in Multi-Disciplinary Engineering Design Conference, Rochester, New York, USA, 2004, p. 04024.

[21] Y. D. Murray, "User’s manual for LS-DYNA concrete material model 159," Federal Highway Administration, FHWA-HRT-05-062, 2007.

[22] A. R. C. Murthy, G. S. Palani, and N. R. Iyer, "Impact Analysis of Concrete Structural Components," vol. 60, pp. 307-319 2010.

[23] N. S. Ottosen, "A failure criterion for concrete," American Society of Civil Engineers. Engineering Mechanics Division. Journal, 1977.

[24] Y. Parfilko and B. Varela, "Simulating Debris Impacts Into Tornado Saferooms with LS-DYNA," Proceedings of Canadian Congress on Applied Mechanics, pp. 339-341, 2015.

[25] Y. Parfilko, B. Varela, and F. Amaral, "Finite Element Analysis of OZ Saferoom," Rochester Institute of Technology, 2015.

[26] L. Petry. “Monographies De Systems D’Artillerie”, Brussels, 1910.

[27] S. Saatci and F. J. Vecchio, "Nonlinear Finite Element Modeling of Reinforced Concrete Structures Under Impact Loads," ACI Structural Journal, vol. 106, pp. 717-725, 2009.

[28] I. S. Sandler and D. Rubin, "An algorithm and a modular subroutine for the CAP model," International Journal for Numerical and Analytical Methods in Geomechanics, vol. 3, pp. 173-186, 1979.

[29] L. Schwer, "An introduction to the Winfrith concrete model," Schwer Engineering & Consulting Services, 2010.

[30] J. A. Teland, "A Review of Empirical Equations for Missile Impact Effects on Concrete," Norwegian Defense Research Establishment, FFI/RAPPORT-97/05856, 1998.

[31] A. K. Vasudevan, "Finite element analysis and experimental comparison of doubly reinforced concrete slabs subjected to blast loads," University of Missouri - Kansas City, 2012.

[32] D. Z. Yankelevsky, "Local Response of Concrete Slabs to Low Velocity Missile Impacts," International Journal of Impact Engineering, vol. 19, pp. 331-343, 1997.

Appendix A. Drawing of Experimental Assembly

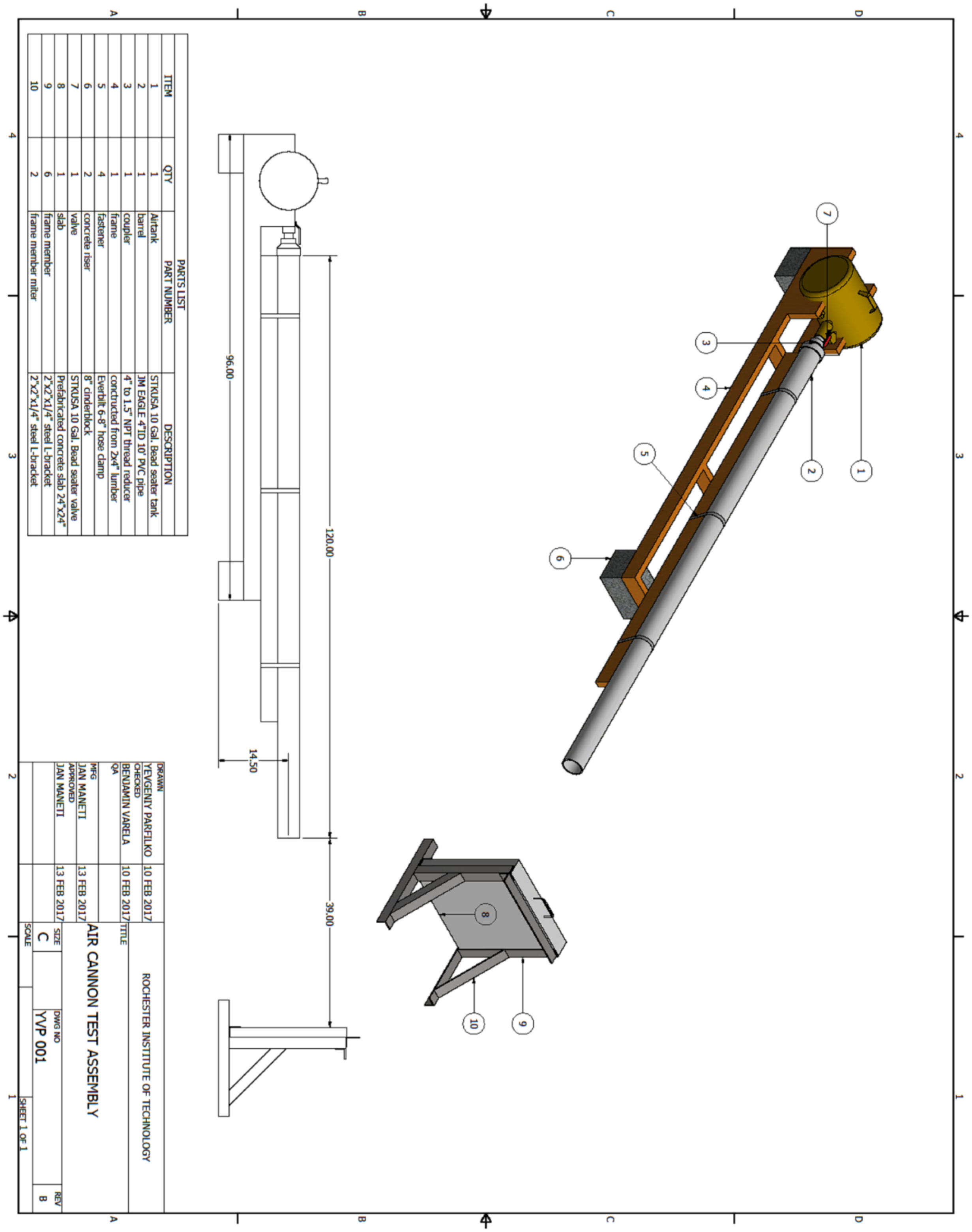

ITEM	QTY	PARTS LIST PART NUMBER	DESCRIPTION
1	1	Airtank	STKUSA 10 Gal. Bead seater tank
2	1	barrel	JM EAGLE 4"ID 10' PVC pipe
3	1	coupler	4" to 1.5" NPT thread reducer
4	1	frame	conctructed from 2x4" lumber
5	4	fastener	Everbilt 6-8" hose clamp
6	2	concrete riser	8" cinderblock
7	1	valve	STKUSA 10 Gal. Bead seater valve
8	1	slab	Prefabricated concrete slab 24"x24"
9	6	frame member	2"x2"x1/4" steel L-bracket
10	2	frame member miter	2"x2"x1/4" steel L-bracket

DRAWN
YEVGENIY PARFILKO 10 FEB 2017
CHECKED
BENJAMIN VARELA 10 FEB 2017
QA
MFG
JAN MANETI 13 FEB 2017
APPROVED
JAN MANETI 13 FEB 2017

ROCHESTER INSTITUTE OF TECHNOLOGY

TITLE
AIR CANNON TEST ASSEMBLY

SIZE C
DWG NO YVP 001
REV B
SCALE
SHEET 1 OF 1

Appendix B. LS-DYNA Input Deck

```
$# LS-DYNA Keyword file created with LS-PrePost(R) V4.3 - 17Feb2017(14:00)
$# Created by Yevgeniy Parfilko, Rochester Institute of Technology
$# Created with ANSYS Workbench v17.2
$# Units: mm, tonne, s, N, K, mJ
$
*KEYWORD
*TITLE
$
$$$$$$$$$$$$$$$$$$$$$$$$$$$$$$$$$$$$$$$$$$$$$$$$$$$$$$$$$$$$$$$$$$$$$$$$$$$$$$$$
$                                CONTROL OPTIONS                               $
$$$$$$$$$$$$$$$$$$$$$$$$$$$$$$$$$$$$$$$$$$$$$$$$$$$$$$$$$$$$$$$$$$$$$$$$$$$$$$$$
$
*CONTROL_ACCURACY
$#     osu       inn    pidosu      iacc
         1         4         0         0
*CONTROL_BULK_VISCOSITY
$#      q1        q2      type     btype
       1.5      0.06        -2         0
*CONTROL_CONTACT
$#  slsfac    rwpnal    islchk    shlthk    penopt    thkchg     orien    enmass
       0.0       0.0         1         1         1         0         2         0
$#  usrstr    usrfrc     nsbcs    interm     xpene     ssthk      ecdt   tiedprj
         0         0         0         0       4.0         0         0         0
$#   sfric     dfric       edc       vfc        th     th_sf    pen_sf
       0.1       0.1      0.01      0.01       0.0       0.0       0.0
$#  ignore    frceng   skiprwg    outseg   spotstp   spotdel   spothin
         1         1         0         1         0         1       0.5
$#    isym    nserod    rwgaps    rwgdth     rwksf      icov    swradf    ithoff
         0         0         1       0.0       1.0         0       0.0         0
$#  shledg    pstiff    ithcnt    tdcnof     ftall    unused    shltrw
         0         0         0         0         0                 0.0
*CONTROL_ENERGY
$#    hgen      rwen    slnten     rylen
         2         1         2         2
*CONTROL_HOURGLASS
$#     ihq        qh
         1       0.1
*CONTROL_SOLID
$#   esort   fmatrix   niptets    swlocl    psfail   t10jtol    icohed    tet13k
         1         0         4         1         0       0.0         0         0
$#   pm1     pm2     pm3     pm4     pm5     pm6     pm7     pm8     pm9    pm10
       0       0       0       0       0       0       0       0       0       0
*CONTROL_TERMINATION
$#  endtim    endcyc     dtmin    endeng    endmas
     0.042  10000000      0.01       5.0       0.0
*CONTROL_TIMESTEP
$#  dtinit    tssfac      isdo    tslimt     dt2ms      lctm     erode     ms1st
       0.0       0.9         0       0.0       0.0         1         1         0
$#  dt2msf   dt2mslc     imscl    unused    unused     rmscl
       0.0         0         0                           0.0
*DATABASE_DEFGEO
$#      dt    binary      lcur     ioopt
      0.01         0         0         1
*DATABASE_ELOUT
$#      dt    binary      lcur     ioopt   option1   option2   option3   option4
1.00000E-4         0         0         1         0         0         0         0
*DAMPING_GLOBAL
$#    lcid    valdmp       stx       sty       stz       srx       sry       srz
         0       0.0       0.0       0.0       0.0       0.0       0.0       0.0
$
$$$$$$$$$$$$$$$$$$$$$$$$$$$$$$$$$$$$$$$$$$$$$$$$$$$$$$$$$$$$$$$$$$$$$$$$$$$$$$$$
$                                 TIME HISTORY                                 $
$$$$$$$$$$$$$$$$$$$$$$$$$$$$$$$$$$$$$$$$$$$$$$$$$$$$$$$$$$$$$$$$$$$$$$$$$$$$$$$$
$
*DATABASE_GLSTAT
$#      dt    binary      lcur     ioopt
3.00000E-5         0         0         1
*DATABASE_MATSUM
```

```
$#      dt    binary      lcur     ioopt
3.00000E-5         0         0         1
*DATABASE_NODOUT
$#      dt    binary      lcur     ioopt   option1   option2
3.00000E-5         0         0         1       0.0         0
*DATABASE_BINARY_D3PLOT
$#      dt      lcdt      beam     npltc    psetid
3.00000E-5         0         0         0         0
$#   ioopt
         0
*DATABASE_BINARY_RUNRSF
$#    cycl        nr      beam     npltc    psetid
    5000.0         0         0         0         0
*DATABASE_EXTENT_BINARY
$#   neiph     neips    maxint    strflg    sigflg    epsflg    rltflg    engflg
         4         6         3         0         1         1         1         1
$#  cmpflg    ieverp    beamip     dcomp      shge     stssz    n3thdt   ialemat
         0         0         0         1         1         1         2         1
$# nintsld   pkp_sen      sclp     hydro     msscl     therm    intout    nodout
         0         0       1.0         0         0         0
$#    dtdt    resplt     neipb
         0         0         0
*DATABASE_FORMAT
$#   iform   ibinary
         2         0
$
$$$$$$$$$$$$$$$$$$$$$$$$$$$$$$$$$$$$$$$$$$$$$$$$$$$$$$$$$$$$$$$$$$$$$$$$$$$$$$$$
$                             BOUNDARY CONDITIONS                              $
$$$$$$$$$$$$$$$$$$$$$$$$$$$$$$$$$$$$$$$$$$$$$$$$$$$$$$$$$$$$$$$$$$$$$$$$$$$$$$$$
$
*BOUNDARY_PRESCRIBED_MOTION_SET_ID
$#      id                                                               heading
$#    nsid       dof       vad      lcid        sf       vid     death     birth
         1Displacement 2
         1         3         2         2       1.0         0       0.0       0.0
         1Displacement
         2         1         2         3       1.0         0       0.0       0.0
         2Displacement
         2         2         2         4       1.0         0       0.0       0.0
$
$$$$$$$$$$$$$$$$$$$$$$$$$$$$$$$$$$$$$$$$$$$$$$$$$$$$$$$$$$$$$$$$$$$$$$$$$$$$$$$$
$                             CONTACT DEFINITIONS                              $
$$$$$$$$$$$$$$$$$$$$$$$$$$$$$$$$$$$$$$$$$$$$$$$$$$$$$$$$$$$$$$$$$$$$$$$$$$$$$$$$
$
$ Contact definition for penalty contact between each projectile and the slab
$
*CONTACT_AUTOMATIC_SINGLE_SURFACE_ID
$#     cid                                                                 title
         0Projectile1 Contact
$#    ssid      msid     sstyp     mstyp    sboxid    mboxid       spr       mpr
         1         0         2         0         0         0         1         0
$#      fs        fd        dc        vc       vdc    penchk        bt        dt
       0.1       0.1      0.01      0.01      0.01         1       0.01.00000E20
$#     sfs       sfm       sst       mst      sfst      sfmt       fsf       vsf
       1.0       1.0       0.0       0.0       1.0       1.0       1.0       1.0
$#    soft    sofscl    lcidab    maxpar     sbopt     depth     bsort    frcfrq
         0       0.1         0     1.025       2.0         2         0         1
*CONTACT_AUTOMATIC_SINGLE_SURFACE_ID
        10Projectile2 Contact
         2         0         2         0         0         0         1         0
       0.1       0.1      0.01      0.01      0.01         1       0.01.00000E20
       1.0       1.0       0.0       0.0       1.0       1.0       1.0       1.0
         0       0.1         0     1.025       2.0         2         0         1
*CONTACT_AUTOMATIC_SINGLE_SURFACE_ID
        11Projectile3 Contact
         3         0         2         0         0         0         1         0
       0.1       0.1      0.01      0.01      0.01         1       0.01.00000E20
       1.0       1.0       0.0       0.0       1.0       1.0       1.0       1.0
         0       0.1         0     1.025       2.0         2         0         1
*CONTACT_AUTOMATIC_SINGLE_SURFACE_ID
        12Projectile4 Contact
```

```
         4         0         2         0         0         0         2         0
       0.1       0.1      0.01      0.01      0.01         1       0.01.00000E20
       1.0       1.0       0.0       0.0       1.0       1.0       1.0       1.0
         0       0.1         0     1.025       2.0         2         0         1
$
$ Contact definition tying endcap nodes to projectile nodes
$
*CONTACT_TIED_NODES_TO_SURFACE_OFFSET
$#     cid                                                                 title
$#    ssid      msid     sstyp     mstyp    sboxid    mboxid       spr       mpr
         3         4         4         0         0         0         0         1
$#      fs        fd        dc        vc       vdc    penchk        bt        dt
       0.0       0.0       0.0       0.0       0.0         0       0.01.00000E20
$#     sfs       sfm       sst       mst      sfst      sfmt       fsf       vsf
       1.0       1.0-1.6660E-4-1.6660E-4       1.0       1.0       1.0       1.0
$#    soft    sofscl    lcidab    maxpar     sbopt     depth     bsort    frcfrq
         0       0.1         0     1.025       3.0         5         0         1
*CONTACT_TIED_NODES_TO_SURFACE_OFFSET
         5         6         4         0         0         0         0         1
       0.0       0.0       0.0       0.0       0.0         0       0.01.00000E20
       1.0       1.0-1.6660E-4-1.6660E-4       1.0       1.0       1.0       1.0
         0       0.1         0     1.025       3.0         5         0         1
*CONTACT_TIED_NODES_TO_SURFACE_OFFSET
         7         8         4         0         0         0         0         1
       0.0       0.0       0.0       0.0       0.0         0       0.01.00000E20
       1.0       1.0-1.6660E-4-1.6660E-4       1.0       1.0       1.0       1.0
         0       0.1         0     1.025       3.0         5         0         1
*CONTACT_TIED_NODES_TO_SURFACE_OFFSET
         9        10         4         0         0         0         0         1
       0.0       0.0       0.0       0.0       0.0         0       0.01.00000E20
       1.0       1.0-1.6660E-4-1.6660E-4       1.0       1.0       1.0       1.0
         0       0.1         0     1.025       3.0         5         0         1
*CONTACT_TIED_NODES_TO_SURFACE_OFFSET
        11        12         4         0         0         0         0         1
       0.0       0.0       0.0       0.0       0.0         0       0.01.00000E20
       1.0       1.0-1.6660E-4-1.6660E-4       1.0       1.0       1.0       1.0
         0       0.1         0     1.025       3.0         5         0         1
*CONTACT_TIED_NODES_TO_SURFACE_OFFSET
        13        14         4         0         0         0         0         1
       0.0       0.0       0.0       0.0       0.0         0       0.01.00000E20
       1.0       1.0-1.6660E-4-1.6660E-4       1.0       1.0       1.0       1.0
         0       0.1         0     1.025       3.0         5         0         1
*CONTACT_TIED_NODES_TO_SURFACE_OFFSET
        15        16         4         0         0         0         0         1
       0.0       0.0       0.0       0.0       0.0         0       0.01.00000E20
       1.0       1.0-1.6660E-4-1.6660E-4       1.0       1.0       1.0       1.0
         0       0.1         0     1.025       3.0         5         0         1
*CONTACT_TIED_NODES_TO_SURFACE_OFFSET
        17        18         4         0         0         0         0         1
       0.0       0.0       0.0       0.0       0.0         0       0.01.00000E20
       1.0       1.0-1.6660E-4-1.6660E-4       1.0       1.0       1.0       1.0
         0       0.1         0     1.025       3.0         5         0         1
$
$ Contact definition constraining rebar within concrete mesh
$
*CONSTRAINED_LAGRANGE_IN_SOLID_TITLE
$#  coupid                                                                 title
         1rebar in slab
$#   slave    master     sstyp     mstyp     nquad     ctype     direc     mcoup
        14         4         1         1         4         2         1         0
$#   start       end      pfac      fric    frcmin      norm   normtyp      damp
       0.01.00000E10       0.1       0.0       0.5         0         0       0.0
$#      cq      hmin      hmax     ileak     pleak   lcidpor     nvent  blockage
       0.0       0.0       0.0         0       0.1         0         0         0
$#  iboxid   ipenchk   intforc   ialesof    lagmul    pfacmm      thkf
         1         0         0         0       0.0         0       0.0
*DEFINE_BOX_TITLE
rebar box
$#   boxid       xmn       xmx       ymn       ymx       zmn       zmx
         1    -320.0     320.0    -320.0     320.0     -50.0      50.0
$
```

```
$$$$$$$$$$$$$$$$$$$$$$$$$$$$$$$$$$$$$$$$$$$$$$$$$$$$$$$$$$$$$$$$$$$$$$$$$$$$$$$$
$                              LIST SET DEFINITIONS                            $
$$$$$$$$$$$$$$$$$$$$$$$$$$$$$$$$$$$$$$$$$$$$$$$$$$$$$$$$$$$$$$$$$$$$$$$$$$$$$$$$
$
*SET_NODE_LIST
$#     sid       da1       da2       da3       da4    solver
         1       0.0       0.0       0.0       0.0MECH
$#    nid1      nid2      nid3      nid4      nid5      nid6      nid7      nid8
     43201     43202     43203     43204     43205     43206     43207     43208
     43211     43212     43213     43214     43215     43216     43209     43210
     43217     43218     43219     43220     43221     43222     43223     43224
     43225     43226     43227     43228     43229     43230     43231     43232
$                              Further nodes redacted for brevity.
*SET_NODE_LIST
         2       0.0       0.0       0.0       0.0MECH
     43201     43202     43203     43204     43205     43206     43207     43208
     43211     43212     43213     43214     43215     43216     43209     43210
     43217     43218     43219     43220     43221     43222     43223     43224
     43225     43226     43227     43228     43229     43230     43231     43232
$                              Further nodes redacted for brevity.
*SET_NODE_LIST
         3       0.0       0.0       0.0       0.0MECH
     46607     46608     46609     46610     46611     46612     46613     46614
     46617     46618     46619     46620     46621     46622     46615     46616
     46623     46624     46625     46626     46627     46628     46629     46630
     46631     46632     46633     46634     46635     46636     46637     46638
$                              Further nodes redacted for brevity.
*SET_SEGMENT
         4       0.0       0.0       0.0       0.0MECH
$#      n1        n2        n3        n4        a1        a2        a3        a4
     51785     51846     51445     51493       0.0       0.0       0.0       0.0
     51784     51857     51846     51785       0.0       0.0       0.0       0.0
     51857     51784     51783     51868       0.0       0.0       0.0       0.0
     51782     51879     51868     51783       0.0       0.0       0.0       0.0
$                              Further data redacted for brevity.
*SET_NODE_LIST
         5       0.0       0.0       0.0       0.0MECH
     46797     46798     46799     46800     46801     46802     46803     46804
     46807     46808     46809     46810     46811     46812     46805     46806
     46813     46814     46815     46816     46817     46818     46819     46820
     46821     46822     46823     46824     46825     46826     46827     46828
$                              Further nodes redacted for brevity.
*SET_SEGMENT
         6       0.0       0.0       0.0       0.0MECH
     56057     56003     55866     55867       0.0       0.0       0.0       0.0
     56056     56007     56003     56057       0.0       0.0       0.0       0.0
     56007     56056     56055     56011       0.0       0.0       0.0       0.0
     56054     56015     56011     56055       0.0       0.0       0.0       0.0
$                              Further data redacted for brevity.
*SET_NODE_LIST
         7       0.0       0.0       0.0       0.0MECH
     46407     46408     46409     46410     46411     46412     46413     46414
     46417     46418     46419     46420     46421     46422     46415     46416
     46423     46424     46425     46426     46427     46428     46429     46430
     46431     46432     46433     46434     46435     46436     46437     46438
$                              Further nodes redacted for brevity.
*SET_SEGMENT
         8       0.0       0.0       0.0       0.0MECH
     55997     56058     55657     55705       0.0       0.0       0.0       0.0
     55996     56069     56058     55997       0.0       0.0       0.0       0.0
     56069     55996     55995     56080       0.0       0.0       0.0       0.0
     55994     56091     56080     55995       0.0       0.0       0.0       0.0
$                              Further data redacted for brevity.
*SET_NODE_LIST
         9       0.0       0.0       0.0       0.0MECH
     47231     47232     47233     47234     47235     47236     47237     47238
     47241     47242     47243     47244     47245     47246     47239     47240
     47247     47248     47249     47250     47251     47252     47253     47254
     47255     47256     47257     47258     47259     47260     47261     47262
$                              Further nodes redacted for brevity.
*SET_SEGMENT
```

```
        10       0.0       0.0       0.0       0.0MECH
     53893     53897     53941     53892       0.0       0.0       0.0       0.0
     53894     53908     53897     53893       0.0       0.0       0.0       0.0
     53908     53894     53895     53919       0.0       0.0       0.0       0.0
     53896     53930     53919     53895       0.0       0.0       0.0       0.0
$                             Further data redacted for brevity.
*SET_NODE_LIST
        11       0.0       0.0       0.0       0.0MECH
     56201     56202     56203     56204     56205     56206     56207     56208
     56211     56212     56213     56214     56215     56216     56209     56210
     56217     56218     56219     56220     56221     56222     56223     56224
     56225     56226     56227     56228     56229     56230     56231     56232
$                             Further nodes redacted for brevity.
*SET_SEGMENT
        12       0.0       0.0       0.0       0.0MECH
     53891     53952     53551     53599       0.0       0.0       0.0       0.0
     53890     53963     53952     53891       0.0       0.0       0.0       0.0
     53963     53890     53889     53974       0.0       0.0       0.0       0.0
     53888     53985     53974     53889       0.0       0.0       0.0       0.0
$                             Further data redacted for brevity.
*SET_NODE_LIST
        13       0.0       0.0       0.0       0.0MECH
     47421     47422     47423     47424     47425     47426     47427     47428
     47431     47432     47433     47434     47435     47436     47429     47430
     47437     47438     47439     47440     47441     47442     47443     47444
     47445     47446     47447     47448     47449     47450     47451     47452
$                             Further nodes redacted for brevity.
*SET_SEGMENT
        14       0.0       0.0       0.0       0.0MECH
     49681     49685     49729     49680       0.0       0.0       0.0       0.0
     49682     49696     49685     49681       0.0       0.0       0.0       0.0
     49696     49682     49683     49707       0.0       0.0       0.0       0.0
     49684     49718     49707     49683       0.0       0.0       0.0       0.0
$                             Further data redacted for brevity.
*SET_NODE_LIST
        15       0.0       0.0       0.0       0.0MECH
     47577     47578     47579     47580     47581     47582     47583     47584
     47587     47588     47589     47590     47591     47592     47585     47586
     47593     47594     47595     47596     47597     47598     47599     47600
     47601     47602     47603     47604     47605     47606     47607     47608
$                             Further nodes redacted for brevity.
*SET_SEGMENT
        16       0.0       0.0       0.0       0.0MECH
     49349     49740     49540     49414       0.0       0.0       0.0       0.0
     49348     49744     49740     49349       0.0       0.0       0.0       0.0
     49744     49348     49347     49748       0.0       0.0       0.0       0.0
     49346     49752     49748     49347       0.0       0.0       0.0       0.0
$                             Further data redacted for brevity.
*SET_NODE_LIST
        17       0.0       0.0       0.0       0.0MECH
     46997     46998     46999     47000     47001     47002     47003     47004
     47007     47008     47009     47010     47011     47012     47005     47006
     47013     47014     47015     47016     47017     47018     47019     47020
     47021     47022     47023     47024     47025     47026     47027     47028
$                             Further nodes redacted for brevity.
*SET_SEGMENT
        18       0.0       0.0       0.0       0.0MECH
     51787     51791     51835     51786       0.0       0.0       0.0       0.0
     51788     51802     51791     51787       0.0       0.0       0.0       0.0
     51802     51788     51789     51813       0.0       0.0       0.0       0.0
     51790     51824     51813     51789       0.0       0.0       0.0       0.0
$                             Further data redacted for brevity.
$
*SET_PART_LIST_TITLE
Projectile1 Set
$#     sid       da1       da2       da3       da4    solver
         1       0.0       0.0       0.0       0.0MECH
$#    pid1      pid2      pid3      pid4      pid5      pid6      pid7      pid8
         1         2         3         4         0         0         0         0
*SET_PART_LIST_TITLE
Projectile2 Set
```

```
         2       0.0       0.0       0.0       0.0MECH
         4         5         6         7         0         0         0         0
*SET_PART_LIST_TITLE
Projectile3 Set
         3       0.0       0.0       0.0       0.0MECH
         4         8         9        10         0         0         0         0
*SET_PART_LIST_TITLE
Projectile4 Set
         4       0.0       0.0       0.0       0.0MECH
         4        11        12        13         0         0         0         0
$
$$$$$$$$$$$$$$$$$$$$$$$$$$$$$$$$$$$$$$$$$$$$$$$$$$$$$$$$$$$$$$$$$$$$$$$$$$$$$$$$
$                              PARTS DEFINITIONS                               $
$$$$$$$$$$$$$$$$$$$$$$$$$$$$$$$$$$$$$$$$$$$$$$$$$$$$$$$$$$$$$$$$$$$$$$$$$$$$$$$$
$
*PART
$#                                                                         title
Cap1B
$#     pid     secid       mid     eosid      hgid      grav    adpopt      tmid
         1         1        98         0         0         0         0         0
*PART
Cap1A
         2         2        98         0         0         0         0         0
*PART
Projectile1
         3         3       143         0         0         0         0         0
*PART
Slab
         4         4       272         0         0         0         0         0
*PART
Cap2B
         5         5        98         0         0         0         0         0
*PART
Cap2A
         6         6        98         0         0         0         0         0
*PART
Projetile2
         7         7       143         0         0         0         0         0
*PART
Cap3B
         8         8        98         0         0         0         0         0
*PART
Cap3A
         9         9        98         0         0         0         0         0
*PART
Projetile3
        10        10       143         0         0         0         0         0
*PART
Cap4B
        11        11        98         0         0         0         0         0
*PART
Cap4A
        12        12        98         0         0         0         0         0
*PART
Projetile4
        13        13       143         0         0         0         0         0
*PART
rebar
        14        14         2         0         0         0         0         0
$
$
$$$$$$$$$$$$$$$$$$$$$$$$$$$$$$$$$$$$$$$$$$$$$$$$$$$$$$$$$$$$$$$$$$$$$$$$$$$$$$$$
$                             SECTION DEFINITIONS                              $
$$$$$$$$$$$$$$$$$$$$$$$$$$$$$$$$$$$$$$$$$$$$$$$$$$$$$$$$$$$$$$$$$$$$$$$$$$$$$$$$
$
*SECTION_SOLID
$#   secid    elform       aet
         1         1         0
*SECTION_SOLID
         2         1         0
*SECTION_SOLID
```

```
         3         1         0
*SECTION_SOLID
         4         1         0
*SECTION_SOLID
         5         1         0
*SECTION_SOLID
         6         1         0
*SECTION_SOLID
         7         1         0
*SECTION_SOLID
         8         1         0
*SECTION_SOLID
         9         1         0
*SECTION_SOLID
        10         1         0
*SECTION_SOLID
        11         1         0
*SECTION_SOLID
        12         1         0
*SECTION_SOLID
        13         1         0
*SECTION_BEAM_TITLE
rebar section
$#   secid    elform      shrf   qr/irid       cst     scoor       nsm
        14         1       1.0         2         1       0.01.00000E-6
$#     ts1       ts2       tt1       tt2     nsloc     ntloc
       3.3       3.3       0.0       0.0       0.0       0.0
$
$$$$$$$$$$$$$$$$$$$$$$$$$$$$$$$$$$$$$$$$$$$$$$$$$$$$$$$$$$$$$$$$$$$$$$$$$$$$$$$$
$                             MATERIAL DEFINITIONS                             $
$$$$$$$$$$$$$$$$$$$$$$$$$$$$$$$$$$$$$$$$$$$$$$$$$$$$$$$$$$$$$$$$$$$$$$$$$$$$$$$$
$
*MAT_ELASTIC_TITLE
rebar steel
$#     mid        ro         e        pr        da        db  not used
         27.85000E-9  200000.0       0.3       0.0       0.0         0
$
*MAT_SIMPLIFIED_JOHNSON_COOK_TITLE
Proectile steel
$#     mid        ro         e        pr        vp
        987.80000E-9  200000.0       0.3       0.0
$#       a         b         n         c    psfail    sigmax    sigsat      epso
    1539.0     477.0      0.18     0.0121.00000E171.00000E281.00000E28       1.0
$
*MAT_WOOD_PINE_TITLE
Projectile Wood
$#     mid        ro     nplot     iters     irate      hard     ifail      ivol
       1435.0000E-10         1         1         1       0.0         0         1
$#    mois      temp    qual_t    qual_c     units     iqual
       0.0      20.0       1.0       1.0         2         0
$#    aopt
       1.0
$#      xp        yp        zp        a1        a2        a3
       0.0       0.0    1000.0       0.0       0.0       0.0
$#      d1        d2        d3
       0.0       0.0       0.0
$
*MAT_RHT_TITLE
RHT Concrete
$#     mid        ro     shear    onempa      epsf        b0        b1        t1
       2722.30000E-9   16000.0      -2.0       2.0       0.0       0.0       0.0
$#       a         n        fc       fs*       ft*        q0         b        t2
       0.0       0.0      32.5      0.18       0.1       0.0       0.0       0.0
$#     e0c       e0t        ec        et     betac     betat       ptf
       0.0       0.0       0.0       0.0       0.0       0.0     0.001
$#     gc*       gt*        xi        d1        d2       epm        af        nf
       0.0       0.0       0.0       0.0       0.0       0.0       0.0       0.0
$#   gamma        a1        a2        a3       pel       pco        np     alpha
       0.0       0.0       0.0       0.0       0.0      35.0       0.0       0.0
$
*MAT_CSCM_CONCRETE_TITLE
```

```
CSCM Concrete
$#     mid        ro     nplot     incre     irate     erode     recov   itretrc
       1592.30000E-9         1       0.0         1       1.1       0.1         0
$#    pred
       0.0
$#     fpc      dagg     units
      32.5      10.0         2
$
*MAT_CONCRETE_DAMAGE_PLASTIC_MODEL_TITLE
CPDM Concrete
$#     mid        ro         e        pr       ecc       qh0        ft        fc
       2732.30000E-9   15600.0       0.2      1.06       0.3      3.25      32.5
$#      hp        ah        bh        ch        dh        as        df       fc0
       0.5      0.08     0.003       2.01.00000E-6      15.0      0.85      10.0
$#    type        bs        wf       wf1       ft1    strflg   failflg       efc
       0.0       1.0      3.25       0.0       0.0       1.0       0.91.00000E-4
$
$$$$$$$$$$$$$$$$$$$$$$$$$$$$$$$$$$$$$$$$$$$$$$$$$$$$$$$$$$$$$$$$$$$$$$$$$$$$$$$$
$                         INITIAL VELOCITY DEFINITIONS                         $
$$$$$$$$$$$$$$$$$$$$$$$$$$$$$$$$$$$$$$$$$$$$$$$$$$$$$$$$$$$$$$$$$$$$$$$$$$$$$$$$
$
*INITIAL_VELOCITY_GENERATION
$#nsid/pid      styp     omega        vx        vy        vz     ivatn      icid
$#      xc        yc        zc        nx        ny        nz     phase    irigid
         1         2       0.0       0.0       0.0  -22000.0         0         0
       0.0       0.0       0.0       0.0       0.0       0.0         0         0
         2         2       0.0       0.0       0.0  -22000.0         0         0
       0.0       0.0       0.0       0.0       0.0       0.0         0         0
         3         2       0.0       0.0       0.0  -22000.0         0         0
       0.0       0.0       0.0       0.0       0.0       0.0         0         0
         5         2       0.0       0.0       0.0  -22000.0         0         0
       0.0       0.0       0.0       0.0       0.0       0.0         0         0
         6         2       0.0       0.0       0.0  -22000.0         0         0
       0.0       0.0       0.0       0.0       0.0       0.0         0         0
         7         2       0.0       0.0       0.0  -22000.0         0         0
       0.0       0.0       0.0       0.0       0.0       0.0         0         0
         8         2       0.0       0.0       0.0  -22000.0         0         0
       0.0       0.0       0.0       0.0       0.0       0.0         0         0
         9         2       0.0       0.0       0.0  -22000.0         0         0
       0.0       0.0       0.0       0.0       0.0       0.0         0         0
        10         2       0.0       0.0       0.0  -22000.0         0         0
       0.0       0.0       0.0       0.0       0.0       0.0         0         0
        11         2       0.0       0.0       0.0  -22000.0         0         0
       0.0       0.0       0.0       0.0       0.0       0.0         0         0
        12         2       0.0       0.0       0.0  -22000.0         0         0
       0.0       0.0       0.0       0.0       0.0       0.0         0         0
        13         2       0.0       0.0       0.0  -22000.0         0         0
       0.0       0.0       0.0       0.0       0.0       0.0         0         0
$
$$$$$$$$$$$$$$$$$$$$$$$$$$$$$$$$$$$$$$$$$$$$$$$$$$$$$$$$$$$$$$$$$$$$$$$$$$$$$$$$
$                               LOAD DEFINITIONS                               $
$$$$$$$$$$$$$$$$$$$$$$$$$$$$$$$$$$$$$$$$$$$$$$$$$$$$$$$$$$$$$$$$$$$$$$$$$$$$$$$$
$
*DEFINE_CURVE
$#    lcid      sidr       sfa       sfo      offa      offo    dattyp     lcint
         1         0       1.0       1.0       0.0       0.0         0         0
$#                a1                  o1
                 0.0   1.0000000000e+008
                0.42   1.0000000000e+008
                 4.2   1.0000000000e+008
*DEFINE_CURVE
         2         0       1.0       1.0       0.0       0.0         0         0
                 0.0                 0.0
                0.42                 0.0
                 4.2                 0.0
*DEFINE_CURVE
         3         0       1.0       1.0       0.0       0.0         0         0
                 0.0                 0.0
                0.42                 0.0
                 4.2                 0.0
*DEFINE_CURVE
```

```
         4         0       1.0       1.0       0.0       0.0         0         0
                 0.0                 0.0
                0.42                 0.0
                 4.2                 0.0
$
$$$$$$$$$$$$$$$$$$$$$$$$$$$$$$$$$$$$$$$$$$$$$$$$$$$$$$$$$$$$$$$$$$$$$$$$$$$$$$$$
$                             ELEMENT DEFINITIONS                              $
$$$$$$$$$$$$$$$$$$$$$$$$$$$$$$$$$$$$$$$$$$$$$$$$$$$$$$$$$$$$$$$$$$$$$$$$$$$$$$$$
$
*ELEMENT_SOLID
$#   eid     pid      n1      n2      n3      n4      n5      n6      n7      n8
       1       4       1   46009   45459   45397   39600   46128   45458   45398
       2       4       1   45397   45459   46009       2   45337   45460   45949
       3       4       2   45337   45460   45949       3   45277   45461   45889
       4       4       3   45277   45461   45889       4   45217   45462   45829
$                             Elements no. 00005-40931 redacted for brevity.
   41052      12   46406   46501   46502   46503   46407   46468   46467   46466
   41053      12   46395   46406   46503   46504   46418   46407   46466   46465
   41054      12   46384   46395   46504   46505   46429   46418   46465   46464
   41055      12   46373   46384   46505   46506   46440   46429   46464   46463
$                             Elements no. 41056-41111 redacted for brevity.
   41112       9   46519   46724   46720   46697   46606   46725   46719   46718
   41113       9   46519   46697   46720   46724   46607   46668   46667   46666
   41114       9   46519   46530   46723   46724   46606   46595   46726   46725
   41115       9   46519   46724   46723   46530   46607   46666   46665   46618
$                             Elements no. 41116-41231 redacted for brevity.
   41232      11   46796   46891   46892   46893   46797   46858   46857   46856
   41233      11   46785   46796   46893   46894   46808   46797   46856   46855
   41234      11   46774   46785   46894   46895   46819   46808   46855   46854
   41235      11   46763   46774   46895   46896   46830   46819   46854   46853
$                             Elements no. 41236-41291 redacted for brevity.
   41292       8   46909   47114   47110   47087   46996   47115   47109   47108
   41293       8   46909   47087   47110   47114   46997   47058   47057   47056
   41294       8   46909   46920   47113   47114   46996   46985   47116   47115
   41295       8   46909   47114   47113   46920   46997   47056   47055   47008
$                             Elements no. 41296-41411 redacted for brevity.
   41412       1   47143   47348   47344   47321   47230   47349   47343   47342
   41413       1   47143   47321   47344   47348   47231   47292   47291   47290
   41414       1   47143   47154   47347   47348   47230   47219   47350   47349
   41415       1   47143   47348   47347   47154   47231   47290   47289   47242
$                             Elements no. 41416-41531 redacted for brevity.
   41532       5   47420   47515   47516   47517   47421   47482   47481   47480
   41533       5   47409   47420   47517   47518   47432   47421   47480   47479
   41534       5   47398   47409   47518   47519   47443   47432   47479   47478
   41535       5   47387   47398   47519   47520   47454   47443   47478   47477
$                             Elements no. 41536-41591 redacted for brevity.
   41592       6   47576   47671   47672   47673   47577   47638   47637   47636
   41593       6   47565   47576   47673   47674   47588   47577   47636   47635
   41594       6   47554   47565   47674   47675   47599   47588   47635   47634
   41595       6   47543   47554   47675   47676   47610   47599   47634   47633
$                             Elements no. 41596-41651 redacted for brevity.
   41652       7   47689   49550   49681   49685   49063   49674   49680   49729
   41653       7   47689   49685   49681   49550   47690   49696   49682   49551
   41654       7   47690   49696   49682   49551   47691   49707   49683   49552
   41655       7   47691   49707   49683   49552   47692   49718   49684   49553
$                             Elements no. 41656-43211 redacted for brevity.
   43212      10   49795   51656   51787   51791   51169   51780   51786   51835
   43213      10   49795   51791   51787   51656   49796   51802   51788   51657
   43214      10   49796   51802   51788   51657   49797   51813   51789   51658
   43215      10   49797   51813   51789   51658   49798   51824   51790   51659
$                             Elements no. 43216-44771 redacted for brevity.
   44772       3   51901   53762   53893   53897   53275   53886   53892   53941
   44773       3   51901   53897   53893   53762   51902   53908   53894   53763
   44774       3   51902   53908   53894   53763   51903   53919   53895   53764
   44775       3   51903   53919   53895   53764   51904   53930   53896   53765
$                             Elements no. 44776-46331 redacted for brevity.
   46332      13   54007   55868   55999   56043   55381   55992   55998   56047
   46333      13   54007   56043   55999   55868   54008   56044   56000   55869
   46334      13   54008   56044   56000   55869   54009   56045   56001   55870
   46335      13   54009   56045   56001   55870   54010   56046   56002   55871
$                             Elements no. 46336-47891 redacted for brevity.
```

```
   47892       2   56113   56318   56314   56291   56200   56319   56313   56312
   47893       2   56113   56291   56314   56318   56201   56262   56261   56260
   47894       2   56113   56124   56317   56318   56200   56189   56320   56319
   47895       2   56113   56318   56317   56124   56201   56260   56259   56212
$                            Elements no. 47896-48011 redacted for brevity.
$
*ELEMENT_BEAM
$#   eid     pid      n1      n2      n3     rt1     rr1     rt2     rr2   local
   48012      14   56347   56348   56349       0       0       0       0       2
   48013      14   56348   56350   56351       0       0       0       0       2
   48014      14   56350   56352   56353       0       0       0       0       2
   48015      14   56352   56354   56355       0       0       0       0       2
$                            Elements no. 48016-48203 redacted for brevity.
$
$$$$$$$$$$$$$$$$$$$$$$$$$$$$$$$$$$$$$$$$$$$$$$$$$$$$$$$$$$$$$$$$$$$$$$$$$$$$$$$$
$                               NODE DEFINITIONS                               $
$$$$$$$$$$$$$$$$$$$$$$$$$$$$$$$$$$$$$$$$$$$$$$$$$$$$$$$$$$$$$$$$$$$$$$$$$$$$$$$$
$
*NODE
$#   nid               x               y               z      tc      rc
       1         294.807         294.807         66.9636       0       0
       2         294.807         294.807         57.7273       0       0
       3         294.807         294.807         48.4909       0       0
       4         294.807         294.807         39.2545       0       0
$                            Nodes no. 00004-56754 redacted for brevity.
$
*END
```